Maximizing the Geometric Mean of User-Rates to Improve Rate-Fairness: Proper vs. Improper Gaussian Signaling

Hongwen Yu, Hoang Duong Tuan, Eryk Dutkiewicz, *Senior Member, IEEE*, H. Vincent Poor, *Life Fellow, IEEE*, and Lajos Hanzo, *Fellow, IEEE*

***Abstract*— This paper considers a reconfigurable intelligent surface (RIS)-aided network, which relies on a multiple antenna array aided base station (BS) and an RIS for serving multiple single antenna downlink users. To provide reliable links to all users over the same bandwidth and same time-slot, the paper proposes the joint design of linear transmit beamformers and the programmable reflecting coefficients of an RIS to maximize the geometric mean (GM) of the users' rates. A new computationally efficient alternating descent algorithm is developed, which is based on closed-forms only for generating improved feasible points of this nonconvex problem. We also consider the joint design of widely linear transmit beamformers and the programmable reflecting coefficients to further improve the GM of the users' rates. Hence another alternating descent algorithm is developed for its solution, which is also based on closed forms only for generating improved feasible points. Numerical examples are provided to demonstrate the efficiency of the proposed approach.**

***Index Terms*— Reconfigurable intelligent surface, proper and improper Gaussian signaling, transmit beamforming, trigonometric function optimization, geometric mean maximization, nonconvex optimization algorithms.**

I. Introduction

The spectral efficiency optimization of wireless networks is often carried out by sum rate (SR) maximization, thanks to the computational tractability of the latter when relying on beamforming [1], [2]. However, by its nature, SR maximization has the deficiency of allocating a large fraction of the sum-rate to a few users having good channel conditions, while leaving the rest of the users with almost zero rates. Furthermore, the SR performance is typically improved with more users involved because there are more flexible choices for the users' channels [3]. The spectral efficiency is thus addressed more appropriately via either SR maximization under specific quality-of-service (QoS) constraints in terms of the users' minimum rate, or by max-min user-rate optimization, but their computation is quite demanding [1], [2], [4]–[6].

Reconfigurable intelligent surfaces (RISs) [7] are constructed by a planar array of programmable reflecting elements (PREs), which have recently been introduced for improving the energy and spectral efficiencies of future wireless networks (6G) [8]–[11], the coverage, reliability and the average achievable rate of UAV communication systems [12]–[14] and the outage probability and bit error rate (BER) of indoor mixed dual-hop VLC/RF systems [15]. Moreover, channel estimation and physical layer security for RIS-aided networks have been studied recently [16]–[19]. A typical RIS-aided system consists of a base station (BS) and a RIS for beneficially reflecting the incident electromagnetic waves from the BS to multi-target directions, where the spectral efficiency may be improved by the joint design of the transmit beamformer at the BS and RIS PREs [20]. The joint design is often based on alternating optimization between the beamformer and PREs. Thus, compared to the design of stand-alone transmit beamformers, the new challenge is the optimization of the PREs with the beamformer weights fixed, which is computationally challenging due to the nonconvex unit-modulus constraint (UMC) imposed on the PREs. In [8] and [21], general-purpose gradient/projected gradient algorithms were used, which do not necessarily converge. By contrast to either convex relaxation relying on dropping the matrix-rank of one constraint or on relaxing the UMC to the convex bounded-by-unit-modulus constraint were used in [22]–[26] for mitigating the computational challenge. Except for the works [22] and [26], which particularly considered the problem of transmit power minimization subject to signal-to-interference-plus-noise ratio (SINR) constraints, all the following treatises [8], [21], [23]–[25] considered the problem of SR maximization. The authors of [23]–[25] applied convex relaxation not only to the UMC but also to the SR objective function. It should be noted that alternating optimization between two sets of decision variables is only efficient, when

Manuscript received November 25, 2020; revised April 19, 2021; accepted July 3, 2021. Date of publication July 14, 2021; date of current version January 10, 2022. This work was supported in part by the Australian Research Councils Discovery Projects under Grant DP190102501, in part by the Engineering and Physical Sciences Research Council through COALESCE under Project EP/P034284/1 and Project EP/P003990/1, and in part by the European Research Council's Advanced Fellow Grant QuantCom under Grant 789028. The associate editor coordinating the review of this article and approving it for publication was M. Payaró. *(Corresponding author: Lajos Hanzo.)*

Hongwen Yu, Hoang Duong Tuan, and Eryk Dutkiewicz are with the School of Electrical and Data Engineering, University of Technology Sydney, Broadway, NSW 2007, Australia (e-mail: hongwen.yu@student.uts.edu.au; tuan.hoang@uts.edu.au; eryk.dutkiewicz@uts.edu.au).

H. Vincent Poor is with the Department of Electrical and Computer Engineering, Princeton University, Princeton, NJ 08544 USA (e-mail: poor@princeton.edu).

Lajos Hanzo is with the School of Electronics and Computer Science, University of Southampton, Southampton SO17 1BJ, U.K. (e-mail: lh@ecs.soton.ac.uk).

Color versions of one or more figures in this article are available at https://doi.org/10.1109/TWC.2021.3095174.

Digital Object Identifier 10.1109/TWC.2021.3095174

the optimization within each set with the other set held fixed is computationally tractable. However that is not the case for the problems considered in all these papers because both the optimization of the beamformers with the PREs held fixed and that of the PREs with the beamformer weights held fixed present difficult nonconvex problems. In the end, the convergence of alternating optimization-based algorithms to a locally optimal solution is not guaranteed. Our recent work [27] has been the first one that addressed the spectral efficiency of RIS-aided communication via max-min user-rate optimization. Instead of alternating optimization, we proposed an alternating descent at the first stage and then a joint descent at the second stage to confirm the optimality of the solutions computed. While the descent iterations in the beamformers generate a sequence of better feasible points, the descent iterations in the PREs generate a sequence of better infeasible points, which converges to a feasible point. Moreover, it has been also shown in [27] that using widely linear beamformers for facilitating improper Gaussian signaling (IGS) improves the users' max-min rate. To sum up, we provide a brief comparison of the related literature in Table I.

Against the above background, this paper offers the following contributions:

- We consider the problem of maximizing the geometric mean (GM) of users' rates for allocating the rates to all users in an equitable manner. We use the users' rate deviation (RD) from their mean and the ratio of the users' maximal and minimal rates (RR) as the main criterion to judge the users' rate balance, which are 0 and 1, respectively, when all users are granted the same rate. The smaller these values are, the fairer the users' rate allocation becomes (more balanced).
- As this problem of GM maximization is computationally intractable, we address it via the min-max joint design of beamforming weights and RIS PREs. To eliminate the UMC of the RIS PREs, we use the polar form of unit-modulus complex numbers that allows each descent iteration of the RIS coefficient calculation to be based on the closed-form solution of an unconstrained nonconvex problem in the PREs' arguments. Each descent iteration of the beamformer weights and the PREs' arguments are also based on the closed-form solutions of convex problems. Thus, the proposed alternating descent method is purely based on closed forms and hence it is computationally efficient.
- Like in [27], here we also use improper Gaussian signaling (IGS) in the BS signal transmission, which has been shown to substantially improve the users' max-min rates (see e.g. [28]–[32]) thanks to its ability to mitigate the severe interferences in interference-limited systems. The performance gap between IGS and conventional proper Gaussian signaling (PGS) becomes substantially wider under more severe interference regimes. To elaborate a little further, IGS is not useful in interference-free regimes such as that of zero-forcing beamforming, which forces all interferences to zero. The interference scenario of SR maximization under PGS is unique in the sense that those users who were allocated zero-rate impose no interference on the other users. As a result, SR maximization under PGS exhibit a high RD and near-infinite RR. Our finding is that compared to PGS, IGS does not improve the system's SR but it results in much lower RD and RR as a benefit of having no users with zero rate. Hence SR maximization becomes a practically feasible option while providing the users with beneficial rate-fairness.

The paper is organized as follows. The joint design of beamformer weights and PREs to maximize the GM of users' rates by tractable computation both under PGS and IGS is addressed in Section II and III, respectively. Their performances are evaluated by the simulations in Section IV, while Section V concludes the paper.

Notation: Only the vector/matrix variables are printed in boldface; I_N is the identity matrix of size $N \times N$, while $O_{M\times N}$ is a zero matrix of size $M \times N$. For $x = (x_1, \ldots, x_n)^T$, $\mathsf{diag}(x)$ is a diagonal matrix of the size $n \times n$ with $x_1, x_2, \ldots, x_n$ on its diagonal; $[X]^2$ is XX^H, and $\langle X, Y\rangle = \mathsf{trace}(X^H Y)$ for the matrices X and Y. Accordingly, the Frobenius norm of X is defined by $||X|| = \sqrt{\mathsf{trace}(X^H X)}$. We also write $\langle X\rangle = \mathsf{trace}(X)$ for notational simplicity. The notation $X \succeq 0$ ($X \succ 0$, resp.) used for the Hermitian symmetric matrix X indicates that it is positive definite (positive semi-definite, resp.). Let us denote the maximal eigenvalue of the Hermitian symmetric matrix X by $\lambda_{\max}(X)$; $\mathsf{vec}(X)$ stacks the columns of the matrix X into a single column (vector) and as such we have $\mathsf{vec}(AXB) = (B^T \otimes A)\mathsf{vec}(X)$ for the matrices A, X, and B of appropriate sizes, where $\otimes$ is the Kronecker product. For a real valued vector $x = (x_1, \ldots, x_n)^T \in \mathbb{R}^n$, $e^{\jmath x}$, $\cos x$, and $\sin x$ are entry-wise understood, i.e. $e^{\jmath x} = (e^{\jmath x_1}, \ldots, e^{\jmath x_n})^T \in \mathbb{C}^n$, $\cos x = (\cos x_1, \ldots, \cos_n)^T \in \mathbb{R}^n$, and $\sin x = (\sin x_1, \ldots, \sin x_n)^T \in \mathbb{R}^n$. As such $e^{\jmath x} = \cos x + \jmath \sin x$. For a complex number x, $\angle x$ denotes its argument, i.e. $x = e^{\jmath \angle x}$ for $|x| = 1$ and it is fully characterized by $\angle x \in [0, 2\pi]$. Lastly, let us denote the set of circular Gaussian random variables with the zero means and variance a by $\mathcal{C}(0, a)$. Each $s \in \mathcal{C}(0, a)$ is termed as being proper because $\mathbb{E}(s^2) = \mathbb{E}(\Re^2\{s\}) - \mathbb{E}(\Im^2\{s\}) = 0$ as $\mathbb{E}(\Re^2\{s\}) = \mathbb{E}(\Im^2\{s\}) = a/2$. By contrast, a Gaussian random vector variable x is referred to as improper if $\mathbb{E}(xx^T) \neq 0$, which particularly implies that $\mathbb{E}(\Re\{x\}\Re^T\{x\}) \neq \mathbb{E}(\Im\{x\}\Im^T\{x\})$.

II. Proper Gaussian Signaling

We consider the RIS-aided communication system illustrated by Fig. 1, where a RIS of N reflecting units supports the downlink spanning from an M-antenna array BS to K single-antenna users (UEs) $k \in \mathcal{K} \triangleq \{1, \ldots, K\}$. Since the RIS is typically deployed on the facade of high-rise buildings and the BS is also usually at a certain elevated height [10], it is justified to assume a LoS link between the BS and RIS, LoS communication between the RIS and UEs, and NLoS propagation between the BS and UEs. Accordingly, the channels spanning from the BS and the RIS to UE k and from the BS to the RIS are modelled by $\tilde{h}_{\text{B-k}} = \sqrt{\beta_{\text{B-k}}} h_{\text{B-k}} \in \mathbb{C}^{1\times M}$, $\tilde{h}_{\text{R-k}} = \sqrt{\beta_{\text{R-k}}} h_{\text{R-k}} \in \mathbb{C}^{1\times N}$, and $\tilde{H}_{\text{B-R}} = \sqrt{\beta_{\text{B-R}}} H_{\text{B-R}} \in \mathbb{C}^{N\times M}$, where $\sqrt{\beta_{\text{B-k}}}$, $\sqrt{\beta_{\text{R-k}}}$, and $\sqrt{\beta_{\text{B-R}}}$ model the path-loss

TABLE I

A Brief Comparison of the Related Literature

Contents \ Literature	**This work**	[27]	[8]	[21]	[22]	[23]	[24]	[25]	[26]
SR maximization	√		√	√		√	√	√	
max-min rate optimization		√							
GM maximization	√								
power minimization					√				√
PGS (linear beamforming)	√	√	√	√	√	√	√	√	√
IGS (widely linear beamforming)	√	√							
trigonometric function optimization	√								
computational tractability in PREs	√	√							

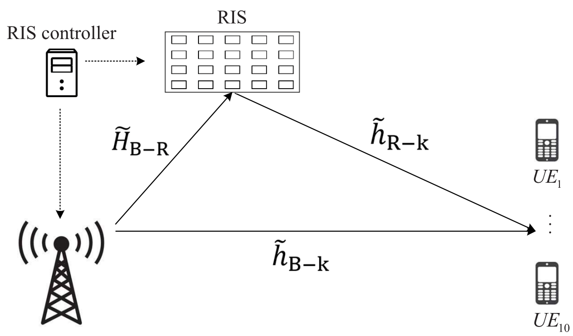

Fig. 1. System model.

and large-scale fading of the BS-to-UE k link, the RIS-to-UE k link, and the BS-to-RIS link, respectively [21], [33], while $h_{\text{R-k}}$ and $H_{\text{B-R}}$ are modelled by Rician fading for modeling the line-of-sight (LoS) channels between the RIS and the UEs as well as between the BS and the RIS [34]. Furthermore, $h_{\text{B-k}}$ is modelled by Rayleigh fading in the face of non-LoS (NLoS) channels between the BS and the UEs. Like many other papers on RIS-aided communication networks, we assume having perfect channel state information, which can be obtained from channel estimation [8], [16], [22].

Let $s_k \in \mathcal{C}(0,1)$ be the information symbol intended for UE k, which is beamformed by $\mathbf{w}_k \in \mathbb{C}^M$. The signal x transmitted from the BS is

$$x = \sum_{k\in\mathcal{K}} \mathbf{w}_k s_k. \tag{1}$$

The signal received at UE k can be expressed as

$$\begin{aligned} y_k &= \left(\tilde{h}_{\text{R-k}}\mathbf{R}_{\text{R-k}}^{1/2}\mathsf{diag}(e^{\jmath\boldsymbol{\theta}})\tilde{H}_{\text{B-R}} + \tilde{h}_{\text{B-k}}\right)x + n_k & (2)\\ &= \mathcal{H}_k(\boldsymbol{\theta})\sum_{k\in\mathcal{K}}\mathbf{w}_k s_k + n_k, & (3)\end{aligned}$$

for

$$\mathcal{H}_k(\boldsymbol{\theta}) \triangleq \tilde{h}_{\text{BR-k}}\mathsf{diag}(e^{\jmath\boldsymbol{\theta}})H_{\text{B-R}} + \tilde{h}_{\text{B-k}} \in \mathbb{C}^{1\times M}, \tag{4}$$

with

$$\tilde{h}_{\text{BR-k}} \triangleq \sqrt{\beta_{\text{B-R}}}\sqrt{\beta_{\text{R-k}}}h_{\text{R-k}}\mathbf{R}_{\text{R-k}}^{1/2} \in \mathbb{C}^{1\times N}, \tag{5}$$

where $\mathbf{R}_{\text{R-k}} \in \mathbb{C}^{N\times N}$ represents the spatial correlation matrix of the RIS elements with respect to user k [21], [35], $n_k \in \mathcal{C}(0,\sigma)$ is the background noise at UE k, and $\mathsf{diag}(e^{\jmath\boldsymbol{\theta}})$ in (2) for $\boldsymbol{\theta} = (\boldsymbol{\theta}_1,\dots,\boldsymbol{\theta}_N)^T \in [0,2\pi]^N$ represents the matrix of PREs.

Let $\mathbf{w} \triangleq \{\mathbf{w}_k, k\in\mathcal{K}\}$. The rate in nats/sec at UE k is

$$r_k(\mathbf{w},\boldsymbol{\theta}) = \ln\left(1 + \frac{|\mathcal{H}_k(\boldsymbol{\theta})\mathbf{w}_k|^2}{\sum_{j\in\mathcal{K}\setminus\{k\}}|\mathcal{H}_k(\boldsymbol{\theta})\mathbf{w}_j|^2 + \sigma}\right). \tag{6}$$

We consider the following problem of jointly designing the beamformers' weight set $\mathbf{w}$ and the PREs $\boldsymbol{\theta}$ to maximize the GM of users' rates:

$$\max_{\mathbf{w},\boldsymbol{\theta}} \left(\prod_{k=1}^{K} r_k(\mathbf{w},\boldsymbol{\theta})\right)^{1/K} \tag{7a}$$

$$\text{s.t.} \sum_{k=1}^{K}||\mathbf{w}_k||^2 \le P, \tag{7b}$$

where (7b) sets the transmit power constraint within a given power budget P. It is plausible that this problem is equivalent to the following one:

$$\min_{\mathbf{w},\boldsymbol{\theta}} f\left(r_1(\mathbf{w},\boldsymbol{\theta}),\dots,r_K(\mathbf{w},\boldsymbol{\theta})\right) \triangleq \frac{1}{\left(\prod_{k=1}^{K} r_k(\mathbf{w},\boldsymbol{\theta})\right)^{1/K}} \quad \text{s.t.} \quad (7b). \tag{8}$$

The function $f(r_1(\mathbf{w},\boldsymbol{\theta}),\dots,r_K(\mathbf{w},\boldsymbol{\theta}))$ is the composition of the convex function $f(r_1,\dots,r_K) = 1/(\prod_{k=1}^K r_k)^{1/K}$ and the non-convex functions $r_k(\mathbf{w},\boldsymbol{\theta})$, $k=1,\dots,K$.

Let $(w^{(\kappa)},\theta^{(\kappa)})$ be a feasible point for (8) that is found from the $(\kappa-1)$-st round. We note that the linearized function of $f\left(r_1(\mathbf{w},\boldsymbol{\theta}),\dots,r_K(\mathbf{w},\boldsymbol{\theta})\right)$ at $\left(r_1(w^{(\kappa)},\theta^{(\kappa)}),\dots,r_K(w^{(\kappa)},\theta^{(\kappa)})\right)$ is

$$2f\Big(r_1(w^{(\kappa)},\theta^{(\kappa)}),\dots,r_K(w^{(\kappa)},\theta^{(\kappa)})\Big) - f(r_1(w^{(\kappa)},\theta^{(\kappa)}),\dots,r_K(w^{(\kappa)},\theta^{(\kappa)}))\frac{1}{K}\sum_{k=1}^{K}\frac{r_k(\mathbf{w},\boldsymbol{\theta})}{r_k(w^{(\kappa)},\theta^{(\kappa)})}. \tag{9}$$

Since we have $f\left(r_1(w^{(\kappa)},\theta^{(\kappa)}),\dots,r_K(w^{(\kappa)},\theta^{(\kappa)})\right) > 0$, we can use steepest descent optimization for the convex function $f(r_1,\dots,r_K)$ to generate the next feasible point $(w^{(\kappa+1)},\theta^{(\kappa+1)})$:

$$\max_{\mathbf{w},\boldsymbol{\theta}} \frac{1}{K}\sum_{k=1}^{K}\frac{r_k(\mathbf{w},\boldsymbol{\theta})}{r_k(w^{(\kappa)},\theta^{(\kappa)})}f(r_1(w^{(\kappa)},\theta^{(\kappa)}),\dots,r_K(w^{(\kappa)},\theta^{(\kappa)}))\text{s.t.} \quad (7b), \tag{10}$$

which is equivalent to the following problem:

$$\max_{\mathbf{w},\boldsymbol{\theta}} f^{(\kappa)}(\mathbf{w},\boldsymbol{\theta}) \triangleq \sum_{k=1}^{K}\gamma_k^{(\kappa)}r_k(\mathbf{w},\boldsymbol{\theta}) \quad \text{s.t.} \quad (7b), \tag{11}$$

for

$$\gamma_k^{(\kappa)} \triangleq \frac{f\left(r_1(w^{(\kappa)},\theta^{(\kappa)}),\dots,r_K(w^{(\kappa)},\theta^{(\kappa)})\right)}{r_k(w^{(\kappa)},\theta^{(\kappa)})}, k=1,\dots,K. \tag{12}$$

A. Beamforming Descent Iteration

To generate $w^{(\kappa+1)}$ we seek $w^{(\kappa+1)}$, so that the following holds:

$$f^{(\kappa)}(w^{(\kappa+1)},\theta^{(\kappa)}) > f^{(\kappa)}(w^{(\kappa)},\theta^{(\kappa)}). \tag{13}$$

Using the inequality [1]

$$\begin{aligned}\ln\left|I_n+[\mathbf{V}]^2(\mathbf{Y})^{-1}\right| &\geq \ln\left|I_n+[\bar{V}]^2(\bar{Y})^{-1}\right|\\ &-\langle[\bar{V}]^2(\bar{Y})^{-1}\rangle+2\Re\{\langle\bar{V}^H(\bar{Y})^{-1}\mathbf{V}\rangle\}\\ &-\langle(\bar{Y})^{-1}-(\bar{Y}+[\bar{V}]^2)^{-1},[\mathbf{V}]^2+\mathbf{Y}\rangle,\\ &\forall\ \mathbf{V},\mathbf{Y}\succ 0\ \ \&\ \ \bar{V},\bar{Y}\succ 0,\end{aligned} \tag{14}$$

for $\mathbf{V}=\mathcal{H}_k(\theta^{(\kappa)})\mathbf{w}_k$, $\mathbf{Y}=\sum_{j\in\mathcal{K}\setminus\{k\}}|\mathcal{H}_k(\theta^{(\kappa)})\mathbf{w}_j|^2+\sigma$, and $\bar{V}=\mathcal{H}_k(\theta^{(\kappa)})w_k^{(\kappa)}$, $\bar{Y}=y_k^{(\kappa)}\triangleq\sum_{j\in\mathcal{K}\setminus\{k\}}|\mathcal{H}_k(\theta^{(\kappa)})w_j^{(\kappa)}|^2+\sigma$, yields

$$\begin{aligned}r_k(\mathbf{w},\theta^{(\kappa)}) &\geq r_k^{(\kappa)}(\mathbf{w})\\ &\triangleq a_k^{(\kappa)}+2\Re\{\langle b_k^{(\kappa)},\mathbf{w}_k\rangle\}\\ &\quad -c_k^{(\kappa)}\sum_{j=1}^K|\mathcal{H}_k(\theta^{(\kappa)})\mathbf{w}_j|^2,\end{aligned} \tag{15}$$

with $a_k^{(\kappa)}\triangleq r_k(w^{(\kappa)},\theta^{(\kappa)})-|\mathcal{H}_k(\theta^{(\kappa)})w_k^{(\kappa)}|^2/y_k^{(\kappa)}-\sigma c_k^{(\kappa)}$, $b_k^{(\kappa)}\triangleq\mathcal{H}_k^H(\theta^{(\kappa)})\mathcal{H}_k(\theta^{(\kappa)})w_k^{(\kappa)}/y_k^{(\kappa)}$, and $0<c_k^{(\kappa)}\triangleq|\mathcal{H}_k(\theta^{(\kappa)})w_k^{(\kappa)}|^2/\left[y_k^{(\kappa)}\left(y_k^{(\kappa)}+|\mathcal{H}_k(\theta^{(\kappa)})w_k^{(\kappa)}|^2\right)\right]$.

The function $r_k^{(\kappa)}(\mathbf{w})$ is seen to be concave quadratic, which matches with $r_k^{(\kappa)}(\mathbf{w},\theta^{(\kappa)})$ at $w^{(\kappa)}$. We solve the following convex problem at the κ-th iteration to generate $w^{(\kappa+1)}$:

$$\max_{\mathbf{w}}\ f_b^{(\kappa)}(\mathbf{w})\quad \text{s.t.}\quad (7b), \tag{16}$$

where

$$\begin{aligned}f_b^{(\kappa)}(\mathbf{w}) &\triangleq \sum_{k=1}^K\gamma_k^{(\kappa)}r_k^{(\kappa)}(\mathbf{w})\\ &=\sum_{k=1}^K\gamma_k^{(\kappa)}a_k^{(\kappa)}+2\sum_{k=1}^K\Re\{\langle\gamma_k^{(\kappa)}b_k^{(\kappa)},\mathbf{w}_k\rangle\}\\ &\quad-\sum_{k=1}^K(\mathbf{w}_k)^H\Psi^{(\kappa)}\mathbf{w}_k\end{aligned} \tag{17}$$

with $0\preceq\Psi^{(\kappa)}\triangleq\sum_{j=1}^K\gamma_j^{(\kappa)}c_j^{(\kappa)}\mathcal{H}_j^H(\theta^{(\kappa)})\mathcal{H}_j(\theta^{(\kappa)})$. By using the Lagrangian multiplier method, we obtain the following closed-form solution of (16)[1]

$$w_k^{(\kappa+1)}=\begin{cases}(\Psi^{(\kappa)})^{-1}\gamma_k^{(\kappa)}b_k^{(\kappa)} \text{if} \sum_{k=1}^K||(\Psi^{(\kappa)})^{-1}\gamma_k^{(\kappa)}b_k^{(\kappa)}||^2\leq P\\ \left(\Psi^{(\kappa)}+\mu I_M\right)^{-1}\gamma_k^{(\kappa)}b_k^{(\kappa)}\quad \text{otherwise,}\end{cases} \tag{18}$$

where $\mu>0$ is chosen by bisection such that $\sum_{k=1}^K||\left(\Psi^{(\kappa)}+\mu I_M\right)^{-1}\gamma_k^{(\kappa)}b_k^{(\kappa)}||^2=P$.

[1] $(\Psi^{(\kappa)})^{-1}$ is understood as the pseudo-inversion when $\Psi^{(\kappa)}\succeq 0$.

B. Programmable Reflecting Elements' Descent Iteration

We seek the next iterative point $\theta^{(\kappa+1)}$ such that

$$f^{(\kappa)}(w^{(\kappa+1)},\theta^{(\kappa+1)}) > f^{(\kappa)}(w^{(\kappa+1)},\theta^{(\kappa)}). \tag{19}$$

Using the inequality (14) for $\mathbf{V}=\mathcal{H}_k(\boldsymbol{\theta})w_k^{(\kappa+1)}$, $\mathbf{Y}=\sum_{j\in\mathcal{K}\setminus\{k\}}|\mathcal{H}_k(\boldsymbol{\theta})w_j^{(\kappa+1)}|^2+\sigma$, and $\bar{V}=\mathcal{H}_k(\theta^{(\kappa)})w_k^{(\kappa+1)}$, $\bar{Y}=y_k^{(\kappa+1)}\triangleq\sum_{j\in\mathcal{K}\setminus\{k\}}|\mathcal{H}_k(\theta^{(\kappa)})w_j^{(\kappa+1)}|^2+\sigma$, yields

$$\begin{aligned}r_k(w^{(\kappa+1)},\boldsymbol{\theta}) &\geq \tilde{r}_k^{(\kappa)}(\boldsymbol{\theta})\\ &\triangleq\frac{2\Re\{(w_k^{(\kappa+1)})^H\mathcal{H}_k^H(\theta^{(\kappa)})\mathcal{H}_k(\boldsymbol{\theta})w_k^{(\kappa+1)}\}}{y_k^{(\kappa+1)}}\\ &\quad+\tilde{a}_k^{(\kappa)}-\tilde{\tilde{c}}_k^{(\kappa)}\sum_{j=1}^K|\mathcal{H}_k(\boldsymbol{\theta})w_j^{(\kappa+1)}|^2,\end{aligned} \tag{20}$$

with $\tilde{a}_k^{(\kappa)}\triangleq r_k(w^{(\kappa+1)},\theta^{(\kappa)})-|\mathcal{H}_k(\theta^{(\kappa)})w_k^{(\kappa+1)}|^2/y_k^{(\kappa+1)}-\sigma\tilde{\tilde{c}}_k^{(\kappa)}$ and $0<\tilde{\tilde{c}}_k^{(\kappa)}\triangleq|\mathcal{H}_k(\theta^{(\kappa)})w_k^{(\kappa+1)}|^2/\left[y_k^{(\kappa+1)}\left(y_k^{(\kappa+1)}+|\mathcal{H}_k(\theta^{(\kappa)})w_k^{(\kappa+1)}|^2\right)\right]$.

Let us define Υ_n as the matrix of size $N\times N$ having only zero entries, except for its (n,n)-entry, which is 1, to express

$$\mathsf{diag}(e^{\jmath\boldsymbol{\theta}})=\sum_{n=1}^N e^{\jmath\boldsymbol{\theta}_n}\Upsilon_n.$$

We then use (4) to arrive at:

$$\begin{aligned}&(w_k^{(\kappa+1)})^H\mathcal{H}_k^H(\theta^{(\kappa)})\mathcal{H}_k(\boldsymbol{\theta})w_k^{(\kappa+1)}\\ &=(w_k^{(\kappa+1)})^H\mathcal{H}_k^H(\theta^{(\kappa)})\left[\tilde{h}_{\text{BR-k}}\mathsf{diag}(e^{\jmath\boldsymbol{\theta}})H_{\text{B-R}}+\tilde{h}_{\text{B-k}}\right]w_k^{(\kappa+1)}\\ &=(w_k^{(\kappa+1)})^H\mathcal{H}_k^H(\theta^{(\kappa)})\tilde{h}_{\text{B-k}}w_k^{(\kappa+1)}\\ &\quad+(w_k^{(\kappa+1)})^H\mathcal{H}_k^H(\theta^{(\kappa)})\tilde{h}_{\text{BR-k}}\mathsf{diag}(e^{\jmath\boldsymbol{\theta}})H_{\text{B-R}}w_k^{(\kappa+1)}\\ &=(w_k^{(\kappa+1)})^H\mathcal{H}_k^H(\theta^{(\kappa)})\tilde{h}_{\text{B-k}}w_k^{(\kappa+1)}\\ &\quad+\sum_{n=1}^N(w_k^{(\kappa+1)})^H\mathcal{H}_k^H(\theta^{(\kappa)})\tilde{h}_{\text{BR-k}}\Upsilon_nH_{\text{B-R}}w_k^{(\kappa+1)}e^{\jmath\boldsymbol{\theta}_n}\\ &=\alpha_k^{(\kappa)}+\sum_{n=1}^N\tilde{b}_k^{(\kappa)}(n)e^{\jmath\theta_n},\end{aligned} \tag{21}$$

with $\alpha_k^{(\kappa)}\triangleq(w_k^{(\kappa+1)})^H\mathcal{H}_k^H(\theta^{(\kappa)})\tilde{h}_{\text{B-k}}w_k^{(\kappa+1)}$, and[2] $\tilde{b}_k^{(\kappa)}(n)=(w_k^{(\kappa+1)})^H\mathcal{H}_k^H(\theta^{(\kappa)})\tilde{h}_{\text{BR-k}}\Upsilon_nH_{\text{B-R}}w_k^{(\kappa+1)}$, $n=1,\dots N$.

To expound further, we have:

$$\begin{aligned}|\mathcal{H}_k(\boldsymbol{\theta})w_j^{(\kappa+1)}|^2 &= \left|\left(\tilde{h}_{\text{BR-k}}\mathsf{diag}(e^{\jmath\boldsymbol{\theta}})H_{\text{B-R}}+\tilde{h}_{\text{B-k}}\right)w_j^{(\kappa+1)}\right|^2\\ &=\left|\tilde{h}_{\text{BR-k}}\mathsf{diag}(e^{\jmath\boldsymbol{\theta}})H_{\text{B-R}}w_j^{(\kappa+1)}\right|^2\\ &\quad+2\Re\{(w_j^{(\kappa+1)})^H\left(\tilde{h}_{\text{B-k}}\right)^H\tilde{h}_{\text{BR-k}}\\ &\quad\mathsf{diag}(e^{\jmath\boldsymbol{\theta}})H_{\text{B-R}}w_j^{(\kappa+1)}\}+|\tilde{h}_{\text{B-k}}w_j^{(\kappa+1)}|^2\\ &=\left|\tilde{h}_{\text{BR-k}}\mathsf{diag}(e^{\jmath\boldsymbol{\theta}})H_{\text{B-R}}w_j^{(\kappa+1)}\right|^2\\ &\quad+2\Re\{\sum_{n=1}^N(w_j^{(\kappa+1)})^H\left(\tilde{h}_{\text{B-k}}\right)^H\tilde{h}_{\text{BR-k}}\Upsilon_n\\ &\quad H_{\text{B-R}}w_j^{(\kappa+1)}e^{\jmath\boldsymbol{\theta}_n}\}+|\tilde{h}_{\text{B-k}}w_j^{(\kappa+1)}|^2.\end{aligned} \tag{22}$$

[2] In what follows $b(i)$ is the i-th entry of b and $[A](i,i)$ is the i-th diagonal entry of A, and $[A]^*(i,i)$ is the complex conjugate of $[A](i,i)$.

Furthermore,

$$\begin{aligned}&\tilde{h}_{\text{BR-k}}\mathsf{diag}(e^{\jmath\boldsymbol{\theta}})H_{\text{B-R}}w_j^{(\kappa+1)}\\&=\tilde{h}_{\text{BR-k}}\left(\sum_{n=1}^{N}e^{\jmath\boldsymbol{\theta}_n}\Upsilon_n\right)H_{\text{B-R}}w_j^{(\kappa+1)}\\&=\sum_{n=1}^{N}\alpha_{k,j}^{(\kappa+1)}(n)e^{\jmath\theta_n},\end{aligned}\tag{23}$$

for $\alpha_{k,j}^{(\kappa+1)}(n)=\tilde{h}_{\text{BR-k}}\Upsilon_n H_{\text{B-R}}w_j^{(\kappa+1)}, n=1,\dots,N$.

Based on (20), (21), (22), and (23), we obtain

$$\begin{aligned}\tilde{r}_k^{(\kappa)}(\boldsymbol{\theta})&=\tilde{a}_k^{(\kappa+1)}+2\Re\{\sum_{n=1}^{N}\tilde{b}_k^{(\kappa)}(n)e^{\jmath\theta_n}\}\\&\quad-\tilde{\tilde{c}}_k^{(\kappa)}\sum_{j=1}^{K}\left|\sum_{n=1}^{N}\alpha_{k,j}^{(\kappa+1)}(n)e^{\jmath\boldsymbol{\theta}_n}\right|^2\\&=\tilde{a}_k^{(\kappa+1)}+2\Re\{\sum_{n=1}^{N}\tilde{b}_k^{(\kappa)}(n)e^{\jmath\theta_n}\}\\&\quad-\tilde{\tilde{c}}_k^{(\kappa)}\sum_{j=1}^{K}(e^{\jmath\boldsymbol{\theta}})^H\Phi_{k,j}^{(\kappa+1)}e^{\jmath\boldsymbol{\theta}},\end{aligned}\tag{24}$$

where $\tilde{a}_k^{(\kappa+1)}\triangleq\tilde{a}_k^{(\kappa)}+2\Re\{\alpha_k^{(\kappa)}\}/y_k^{(\kappa+1)}-\tilde{\tilde{c}}_k^{(\kappa)}\sum_{j=1}^{N}|\tilde{h}_{\text{B-k}}w_j^{(\kappa+1)}|^2$, $\tilde{b}_k^{(\kappa+1)}(n)\triangleq\tilde{b}_k^{(\kappa)}(n)/y_k^{(\kappa+1)}-\tilde{\tilde{c}}_k^{(\kappa)}\sum_{j=1}^{K}(w_j^{(\kappa+1)})^H\left(\tilde{h}_{\text{B-k}}\right)^H\tilde{h}_{\text{BR-k}}\Upsilon_n H_{\text{B-R}}w_j^{(\kappa+1)}$, and $\Phi_{k,j}^{(\kappa+1)}(n,m)=(\alpha_{k,j}^{(\kappa+1)}(n))^*\alpha_{k,j}^{(\kappa+1)}(m), n=1,\dots,N; m=1,\dots,N$.

Note that $\Phi_{k,j}^{(\kappa+1)}\succeq 0$. Therefore,

$$\begin{aligned}f_c^{(\kappa)}(\boldsymbol{\theta})&\triangleq\sum_{k=1}^{K}\gamma_k^{(\kappa)}\tilde{r}_k^{(\kappa)}(\boldsymbol{\theta})\\&=\tilde{a}^{(\kappa+1)}+2\Re\{\sum_{n=1}^{N}\tilde{b}^{(\kappa+1)}(n)e^{\jmath\theta_n}\}\\&\quad-(e^{\jmath\boldsymbol{\theta}})^H\Phi^{(\kappa+1)}e^{\jmath\boldsymbol{\theta}},\end{aligned}\tag{25}$$

for $\tilde{a}^{(\kappa+1)}\triangleq\sum_{k=1}^{K}\gamma_k^{(\kappa)}\tilde{a}_k^{(\kappa+1)}$, $\tilde{b}^{(\kappa+1)}(n)\triangleq\sum_{k=1}^{K}\gamma_k^{(\kappa)}\tilde{b}_k^{(\kappa+1)}(n), n=1,\dots,N$, and $0\preceq\Phi^{(\kappa+1)}\triangleq\sum_{k=1}^{K}\sum_{j=1}^{N}\gamma_k^{(\kappa)}\tilde{\tilde{c}}_k^{(\kappa)}\Phi_{k,j}^{(\kappa+1)}$.

We use the following problem at the κ-th iteration to generate $\theta^{(\kappa+1)}$:

$$\max_{\boldsymbol{\theta}}\ f_c^{(\kappa)}(\boldsymbol{\theta}).\tag{26}$$

Following [36], we have (27), as shown at the bottom of the page.

We thus solve the following problem at the κ-th iteration to generate $\theta^{(\kappa+1)}$:

$$\max_{\boldsymbol{\theta}}\ \tilde{f}_c^{(\kappa)}(\boldsymbol{\theta}),\tag{28}$$

where the function $\tilde{f}_c^{(\kappa)}(\boldsymbol{\theta})$ is an affine function of $e^{\jmath\boldsymbol{\theta}}$. By noting that $\Re\{ce^{\jmath\theta_n}\}=|c|\cos(\angle c+\theta_n)$ and thus it is maximized at $\theta_n=-\angle c$, we obtain the closed-form solution of (28) as[3]

$$\begin{aligned}\theta_n^{(\kappa+1)}=-\angle(&\tilde{b}^{(\kappa+1)}(n)-\sum_{m=1}^{N}e^{-\jmath\theta_m^{(\kappa)}}\Phi^{(\kappa+1)}(m,n)\\&+\lambda_{\max}(\Phi^{(\kappa+1)})e^{-\jmath\theta_n^{(\kappa)}}), n=1,\dots,N.\end{aligned}\tag{29}$$

It follows from (27) that $f^{(\kappa)}(w^{(\kappa+1)},\theta^{(\kappa+1)})\geq f_c^{(\kappa)}(\theta^{(\kappa+1)})\geq\tilde{f}_c^{(\kappa)}(\theta^{(\kappa+1)})>\tilde{f}_c^{(\kappa)}(\theta^{(\kappa)})=f_c^{(\kappa)}(\theta^{(\kappa)})=f^{(\kappa)}(w^{(\kappa+1)},\theta^{(\kappa)})$, confirming (19), so $\theta^{(\kappa+1)}$ is a better feasible point than $\theta^{(\kappa)}$.

C. Proper Gaussian Signaling Geometric Mean Rate Optimization

Algorithm 1 provides the pseudo-code for the proposed computational procedure of steepest descent for computing (9) as the iterations (18) and (29) seek a descent direction by seeking a better feasible point for the nonconvex problem (10) instead of seeking its optimal solution for reducing the computational load with guaranteed convergence, as it is often

[3] $[(\Phi^{(\kappa+1)}-\mu I_N)e^{\jmath\theta^{(\kappa)}}](n)$ is the n-th entry of $(\Phi^{(\kappa+1)}-\mu I_N)e^{\jmath\theta^{(\kappa)}}$.

$$\begin{aligned}f_c^{(\kappa)}(\boldsymbol{\theta})&=\tilde{a}^{(\kappa+1)}+2\Re\{\sum_{n=1}^{N}\tilde{b}^{(\kappa+1)}(n)e^{\jmath\theta_n}\}-(e^{\jmath\boldsymbol{\theta}})^H(\Phi^{(\kappa+1)}-\lambda_{\max}(\Phi^{(\kappa+1)})I_N)e^{\jmath\boldsymbol{\theta}}-\lambda_{\max}(\Phi^{(\kappa+1)})(e^{\jmath\boldsymbol{\theta}})^H I_N e^{\jmath\boldsymbol{\theta}}\\&=\tilde{a}^{(\kappa+1)}+2\Re\{\sum_{n=1}^{N}\tilde{b}^{(\kappa+1)}(n)e^{\jmath\theta_n}\}-(e^{\jmath\boldsymbol{\theta}})^H(\Phi^{(\kappa+1)}-\lambda_{\max}(\Phi^{(\kappa+1)})I_N)e^{\jmath\boldsymbol{\theta}}-\lambda_{\max}(\Phi^{(\kappa+1)})N\\&\geq\tilde{f}_c^{(\kappa)}(\boldsymbol{\theta})\\&\triangleq\tilde{a}^{(\kappa+1)}+2\Re\{\sum_{n=1}^{N}\tilde{b}^{(\kappa+1)}(n)e^{\jmath\theta_n}\}-[2\Re\{(e^{\jmath\theta^{(\kappa)}})^H(\Phi^{(\kappa+1)}-\lambda_{\max}(\Phi^{(\kappa+1)})I_N)e^{\jmath\boldsymbol{\theta}}\}\\&\quad-(e^{\jmath\theta^{(\kappa)}})^H(\Phi^{(\kappa+1)}-\lambda_{\max}(\Phi^{(\kappa+1)})I_N)e^{\jmath\theta^{(\kappa)}}]-\lambda_{\max}(\Phi^{(\kappa+1)})N\\&=\tilde{a}^{(\kappa+1)}+2\Re\{\sum_{n=1}^{N}(\tilde{b}^{(\kappa+1)}(n)-\sum_{m=1}^{N}e^{-\jmath\theta_m^{(\kappa)}}\Phi^{(\kappa+1)}(m,n)+\lambda_{\max}(\Phi^{(\kappa+1)})e^{-\jmath\theta_n^{(\kappa)}})e^{\jmath\theta_n}\}\\&\quad-(e^{\jmath\theta^{(\kappa)}})^H\Phi^{(\kappa+1)}e^{\jmath\theta^{(\kappa)}}-2\lambda_{\max}(\Phi^{(\kappa+1)})N.\end{aligned}\tag{27}$$

Algorithm 1 PGS GM Descent Algorithm

1: **Initialization:** Set $\kappa = 0$. Randomly generate $(w^{(0)}, \theta^{(0)})$ satisfying the constraint (7b) and define $\gamma^{(0)}$ by (12).
2: **Repeat until convergence of the objective in** (8)**:** Generate $w^{(\kappa+1)}$ by (18) and $\theta^{(\kappa+1)}$ by (29). Reset $\kappa \leftarrow \kappa + 1$.
3: **Output** $(w^{(\kappa)}, \theta^{(\kappa)})$ and rates $r_k(w^{(\kappa)}, \theta^{(\kappa)})$, $k = 1, \ldots, K$ with their GM $\left(\prod_{k=1}^{K} r_k(w^{(\kappa)}, \theta^{(\kappa)})\right)^{1/K}$.

done in the context of the Frank-and-Wolfe method [37]. Of course, one can still seek the optimal solution of (10) for the steepest descent by iterating (18) and (29) many times, because according to [27], this kind of alternating descent iterations often converge to at least a locally optimal solution of (10). The global optimality cannot be proved theoretically, but we found that it is globally optimal in many cases.

To the best of our knowledge, there is no the conventional descent algorithm, because the conception of descent algorithms is a research branch in computational optimization and what make descent algorithms different is the specific way they choose their a descent directions. Hence, our descent directions are completely new and rather different from the popular steepest descent techniques. Furthermore, all other exiting algorithms, which solve convex problems and iteratively at a high complexity are very sensitive to the problem sizes. However, our algorithms iterate using closed- form expressions, hence their complexity is low.

III. Improper Gaussian Signaling

In (1), the proper Gaussian sources s_k are linearly beamformed by the beamformers $\mathbf{w}_k$, hence the transmit signal x is also proper Gaussian, i.e. $\mathbb{E}(xx^T) = \sum_{k\in\mathcal{K}} \mathbf{w}_k(\mathbf{w}_k)^T \mathbb{E}[(s_k)^2] = 0$. In this section, the proper Gaussian sources s_k are widely linearly beamformed by the pairs of beamformers $\mathbf{w}_{1,k} \in \mathbb{C}^M$ and $\mathbf{w}_{2,k} \in \mathbb{C}^M$ as in [38]

$$\begin{bmatrix}\mathbf{w}_{1,k} & \mathbf{w}_{2,k}\end{bmatrix}\begin{bmatrix}s_k\\ s_k^*\end{bmatrix}, \tag{30}$$

resulting in the transmit signal

$$x = \sum_{k=1}^{K}(\mathbf{w}_{1,k}s_k + \mathbf{w}_{2,k}s_k^*), \tag{31}$$

and for improper Gaussian, as

$$\mathbb{E}(xx^T) = \sum_{k=1}^{K}(\mathbf{w}_{1,k}\mathbf{w}_{2,k}^T + \mathbf{w}_{2,k}\mathbf{w}_{1,k}^T)\mathbb{E}(|s_k|^2) \neq 0.$$

The equation (2) of the received signal at UE k becomes:

$$y_k = \mathcal{H}_k(\boldsymbol{\theta})\sum_{k=1}^{K}(\mathbf{w}_{1,k}s_k + \mathbf{w}_{2,k}s_k^*) + n_k. \tag{32}$$

We augment (32) as

$$\begin{aligned}\begin{bmatrix}y_k\\ y_k^*\end{bmatrix} &= \begin{bmatrix}\mathcal{H}_k(\boldsymbol{\theta}) & 0\\ 0 & \mathcal{H}_k^*(\boldsymbol{\theta})\end{bmatrix}\sum_{k=1}^{K}\begin{bmatrix}\mathbf{w}_{1,k} & \mathbf{w}_{2,k}\\ \mathbf{w}_{2,k}^* & \mathbf{w}_{1,k}^*\end{bmatrix}\begin{bmatrix}s_k\\ s_k^*\end{bmatrix} + \begin{bmatrix}n_k\\ n_k^*\end{bmatrix}\\ &= \Lambda_k(\boldsymbol{\theta})\sum_{k=1}^{K}\mathbf{W}_k\bar{s}_k + \bar{n}_k,\end{aligned} \tag{33}$$

for the linear mappings $\Lambda_k(\boldsymbol{\theta}) \triangleq \begin{bmatrix}\mathcal{H}_k(\boldsymbol{\theta}) & 0\\ 0 & \mathcal{H}_k^*(\boldsymbol{\theta})\end{bmatrix} \in \mathbb{C}^{2\times(2M)}$, and $\mathbf{W}_k \triangleq \begin{bmatrix}\mathbf{w}_{1,k} & \mathbf{w}_{2,k}\\ \mathbf{w}_{2,k}^* & \mathbf{w}_{1,k}^*\end{bmatrix} \in \mathbb{C}^{2M\times 2}$, and $\bar{s}_k \triangleq \begin{bmatrix}s_k\\ s_k^*\end{bmatrix} \in \mathbb{C}^2$, $\bar{n}_k \triangleq \begin{bmatrix}n_k\\ n_k^*\end{bmatrix} \in \mathbb{C}^2$.

For $\mathbf{w} \triangleq \{\mathbf{w}_k \triangleq \begin{bmatrix}\mathbf{w}_{1,k}\\ \mathbf{w}_{2,k}\end{bmatrix} \in \mathbb{C}^{2M} : k \in \mathcal{K}\}$, the rate at UE k is calculated by $(1/2)r_k(\mathbf{w},\boldsymbol{\theta})$ [39] with

$$r_k(\mathbf{w},\boldsymbol{\theta}) = \ln\left|I_2 + [\Lambda_k(\boldsymbol{\theta})\mathbf{W}_k]^2 \left(\sum_{j\in\mathcal{K}\setminus\{k\}}[\Lambda_k(\boldsymbol{\theta})\mathbf{W}_j]^2 + \sigma I_2\right)^{-1}\right|. \tag{34}$$

For the particular class of $\mathbf{w}_{2,k} \equiv 0$, i.e. when x in (31) is proper Gaussian, it may be shown that

$$r_k(\mathbf{w},\boldsymbol{\theta}) = 2\ln\left(1 + |\mathcal{H}_k(\boldsymbol{\theta})\mathbf{w}_{1,k}|^2/(\sum_{j\in\mathcal{K}\setminus\{k\}}|\mathcal{H}_k(\boldsymbol{\theta})\mathbf{w}_{1,j}|^2 + \sigma)\right),$$

hence $(1/2)r_k(\mathbf{w},\boldsymbol{\theta})$ is the known rate (6).

Like (8), the problem of maximizing the GM for users' rates corresponding IGS is thus formulated as

$$\min_{\mathbf{w},\boldsymbol{\theta}} f\left(r_1(\mathbf{w},\boldsymbol{\theta}),\ldots,r_K(\mathbf{w},\boldsymbol{\theta})\right) \triangleq \frac{1}{\left(\prod_{k=1}^{K} r_k(\mathbf{w},\boldsymbol{\theta})\right)^{1/K}} \tag{35a}$$

$$\text{s.t.} \sum_{k=1}^{K}(||\mathbf{w}_{1,k}||^2 + ||\mathbf{w}_{2,k}||^2) \leq P. \tag{35b}$$

Let $(w^{(\kappa)}, \theta^{(\kappa)})$ be a feasible point for (35) that is found from the $(\kappa-1)$-st round. Like (11), we use the following steepest descent optimization for the convex function $f(r_1,\ldots,r_K) = 1/(\prod_{k=1}^{K} r_k)^{1/K}$ to generate the next feasible point $(w^{(\kappa+1)}, \theta^{(\kappa+1)})$:

$$\max_{\mathbf{w},\boldsymbol{\theta}} F^{(\kappa)}(\mathbf{w},\boldsymbol{\theta}) \triangleq \sum_{k=1}^{K}\gamma_k^{(\kappa)} r_k(\mathbf{w},\boldsymbol{\theta}) \quad \text{s.t.} \quad (35b) \tag{36}$$

where

$$\gamma_k^{(\kappa)} \triangleq \frac{f\left(r_1(w^{(\kappa)},\theta^{(\kappa)}),\ldots,r_K(w^{(\kappa)},\theta^{(\kappa)})\right)}{r_k(w^{(\kappa)},\theta^{(\kappa)})}, k = 1,\ldots,K. \tag{37}$$

Another way of defining the UEs' rates is through the equivalent composite real system for (32):

$$\begin{aligned}\tilde{y}_k &\triangleq \begin{bmatrix}\Re\{y_k\}\\ \Im\{y_k\}\end{bmatrix}\\ &= \begin{bmatrix}\Re\{\mathcal{H}_k(\boldsymbol{\theta})\} - \Im\{\mathcal{H}_k(\boldsymbol{\theta})\}\\ \Im\{\mathcal{H}_k(\boldsymbol{\theta})\}\Re\{\mathcal{H}_k(\boldsymbol{\theta})\}\end{bmatrix}\\ &\sum_{j=1}^{K}\begin{bmatrix}\Re\{\mathbf{w}_{1,j}\} + \Re\{\mathbf{w}_{2,j}\} - \Im\{\mathbf{w}_{1,j}\} + \Im\{\mathbf{w}_{2,j}\}\\ \Im\{\mathbf{w}_{1,j}\} + \Im\{\mathbf{w}_{2,j}\}\Re\{\mathbf{w}_{1,j}\} - \Re\{\mathbf{w}_{2,j}\}\end{bmatrix}\end{aligned}$$

$$\times \begin{bmatrix}\Re\{s_j\}\\ \Im\{s_j\}\end{bmatrix} + \begin{bmatrix}\Re\{n_k\}\\ \Im\{n_k\}\end{bmatrix}$$
$$= \bar{\mathcal{H}}_k(\boldsymbol{\theta})\sum_{j=1}^{K}\mathbf{V}_j\tilde{s}_j + \tilde{n}_k, \tag{38}$$

where we have:

$$\bar{\mathcal{H}}_k(\boldsymbol{\theta}) \triangleq \begin{bmatrix}\Re\{\mathcal{H}_k(\boldsymbol{\theta})\} & -\Im\{\mathcal{H}_k(\boldsymbol{\theta})\}\\ \Im\{\mathcal{H}_k(\boldsymbol{\theta})\} & \Re\{\mathcal{H}_k(\boldsymbol{\theta})\}\end{bmatrix}, \tilde{s}_j \triangleq \begin{bmatrix}\Re\{s_j\}\\ \Im\{s_j\}\end{bmatrix}, \tag{39}$$
$$\mathbf{V}_j \triangleq \begin{bmatrix}\mathbf{v}_j^{11} & \mathbf{v}_j^{12}\\ \mathbf{v}_j^{21} & \mathbf{v}_j^{22}\end{bmatrix}, \tilde{n}_k = \begin{bmatrix}\Re\{n_k\}\\ \Im\{n_k\}\end{bmatrix}, \tag{40}$$

under the following transformation:

$$\begin{bmatrix}\Re\{\mathbf{w}_{1,j}\}+\Re\{\mathbf{w}_{2,j}\} & -\Im\{\mathbf{w}_{1,j}\}+\Im\{\mathbf{w}_{2,j}\}\\ \Im\{\mathbf{w}_{1,j}\}+\Im\{\mathbf{w}_{2,j}\} & \Re\{\mathbf{w}_{1,j}\}-\Re\{\mathbf{w}_{2,j}\}\end{bmatrix} = \mathbf{V}_j. \tag{41}$$

This transform is indeed legitimate, since its inverse is given by

$$\begin{bmatrix}\Re\{\mathbf{w}_{1,j}\} & \Im\{\mathbf{w}_{1,j}\}\\ \Re\{\mathbf{w}_{2,j}\} & \Im\{\mathbf{w}_{2,j}\}\end{bmatrix} = \frac{1}{2}\begin{bmatrix}\mathbf{v}_j^{11}+\mathbf{v}_j^{22} & \mathbf{v}_j^{21}-\mathbf{v}_j^{12}\\ \mathbf{v}_j^{11}-\mathbf{v}_j^{22} & \mathbf{v}_j^{21}+\mathbf{v}_j^{12}\end{bmatrix}. \tag{42}$$

Furthermore, we have:

$$||\mathbf{w}_j||^2 = \frac{1}{2}\sum_{i=1}^{2}\sum_{\ell=1}^{2}||\mathbf{v}_j^{i\ell}||^2, \tag{43}$$

hence the power constraint (35b) for $\mathbf{w}$ is transferred to the following constraint

$$\sum_{j=1}^{K}||\mathbf{v}_j||^2 \le 2P \tag{44}$$

for

$$\mathbf{v}_j \triangleq \mathsf{vec}(\mathbf{V}_j) = \begin{bmatrix}\mathbf{v}_j^{11}\\ \mathbf{v}_j^{21}\\ \mathbf{v}_j^{12}\\ \mathbf{v}_j^{22}\end{bmatrix}. \tag{45}$$

For $\mathbf{v} \triangleq \{\mathbf{v}_j, j\in\mathcal{K}\}$, the problem (36) is equivalent to the problem

$$\max_{\mathbf{v},\boldsymbol{\theta}} \tilde{F}^{(\kappa)}(\mathbf{v},\boldsymbol{\theta}) \triangleq \sum_{k=1}^{K}\gamma_k^{(\kappa)}\tilde{r}_k(\mathbf{v},\boldsymbol{\theta}) \quad \text{s.t.} \quad (44) \tag{46}$$

with

$$\tilde{r}_k(\mathbf{v},\boldsymbol{\theta}) = \ln\left|I_2 + [\bar{\mathcal{H}}_k(\boldsymbol{\theta})\mathbf{V}_k]^2 \left(\sum_{j\in\mathcal{K}\setminus\{k\}}[\bar{\mathcal{H}}_k(\boldsymbol{\theta})\mathbf{V}_j]^2 + \sigma I_2\right)^{-1}\right|. \tag{47}$$

We propose the following alternating descent iterations at the κ-th round to generate a better feasible point $(w^{(\kappa+1)}, \theta^{(\kappa+1)})$.

A. Widely Linear Beamforming Descent Iteration

We seek $w^{(\kappa+1)}$ such that

$$F^{(\kappa)}(w^{(\kappa+1)},\theta^{(\kappa)}) > F^{(\kappa)}(w^{(\kappa)},\theta^{(\kappa)}). \tag{48}$$

Upon using (41) to define

$$V_j^{(\kappa)} \triangleq \begin{bmatrix}\Re\{w_{1,j}^{(\kappa)}\}+\Re\{w_{2,j}^{(\kappa)}\} & -\Im\{w_{1,j}^{(\kappa)}\}+\Im\{w_{2,j}^{(\kappa)}\}\\ \Im\{w_{1,j}^{(\kappa)}\}+\Im\{w_{2,j}^{(\kappa)}\} & \Re\{w_{1,j}^{(\kappa)}\}-\Re\{w_{2,j}^{(\kappa)}\}\end{bmatrix} \tag{49}$$

we have $v_j^{(\kappa)} \triangleq \mathsf{vec}(V_j^{(\kappa)})$.

By using the inequality (14) for $\mathbf{V} = \bar{\mathcal{H}}_k(\theta^{(\kappa)})\mathbf{V}_k$, $\mathbf{Y} = \sum_{j\in\mathcal{K}\setminus\{k\}}[\bar{\mathcal{H}}_k(\theta^{(\kappa)})\mathbf{V}_j]^2 + \sigma I_2$, and $\bar{V} = \bar{\mathcal{H}}_k(\theta^{(\kappa)})V_k^{(\kappa)}$, $\bar{Y} = Y_k^{(\kappa)} \triangleq \sum_{j\in\mathcal{K}\setminus\{k\}}[\bar{\mathcal{H}}_k(\theta^{(\kappa)})V_j^{(\kappa)}]^2 + \sigma I_2 \succeq 0$, we obtain the following concave quadratic lower bounding function approximation of $\tilde{r}_k(\theta^{(\kappa)},\mathbf{v})$:

$$\tilde{r}_k(\mathbf{v},\theta^{(\kappa)}) \ge \tilde{r}_k^{(\kappa)}(\mathbf{v})$$
$$\triangleq a_k^{(\kappa)} + 2\langle B_k^{(\kappa)}\mathbf{V}_k\rangle - \langle C_k^{(\kappa)}, \sum_{j\in\mathcal{K}}[\bar{\mathcal{H}}_k(\theta^{(\kappa)})\mathbf{V}_j]^2\rangle, \tag{50}$$

with $a_k^{(\kappa)} \triangleq \tilde{r}_k(v^{(\kappa)},\theta^{(\kappa)}) - \langle[\bar{\mathcal{H}}_k(\theta^{(\kappa)})V_k^{(\kappa)}]^2(Y_k^{(\kappa)})^{-1}\rangle - \sigma\langle C_k^{(\kappa)}\rangle$, $B_k^{(\kappa)} \triangleq (V_k^{(\kappa)})^H(\bar{\mathcal{H}}_k(\theta^{(\kappa)}))^t(Y_k^{(\kappa)})^{-1} \times \bar{\mathcal{H}}_k(\theta^{(\kappa)})$, and $0 \prec C_k^{(\kappa)} \triangleq (Y_k^{(\kappa)})^{-1} - \left(Y_k^{(\kappa)} + [\bar{\mathcal{H}}_k(\theta^{(\kappa)})V_k^{(\kappa)}]^2\right)^{-1}$.

Note that $\langle B_k^{(\kappa)}\mathbf{V}_k\rangle = \langle\mathsf{vec}((B_k^{(\kappa)})^T),\mathbf{v}_k\rangle$, and

$$\begin{aligned}&\langle C_k^{(\kappa)}, [\bar{\mathcal{H}}_k(\theta^{(\kappa)})\mathbf{V}_j]^2\rangle\\ &= ||\mathsf{vec}\left((C_k^{(\kappa)})^{1/2}\bar{\mathcal{H}}_k(\theta^{(\kappa)})\mathbf{V}_j\right)||^2\\ &= ||\left(I_2\otimes((C_k^{(\kappa)})^{1/2}\bar{\mathcal{H}}_k(\theta^{(\kappa)}))\right)\mathsf{vec}(\mathbf{V}_j)||^2\\ &= \mathsf{vec}^T(\mathbf{V}_j)\left[I_2\otimes\left(\bar{\mathcal{H}}_k^T(\theta^{(\kappa)})C_k^{(\kappa)}\bar{\mathcal{H}}_k(\theta^{(\kappa)})\right)\right]\mathsf{vec}(\mathbf{V}_j)\\ &= \mathbf{v}_j^T\mathcal{Q}_k^{(\kappa)}\mathbf{v}_j\end{aligned}$$

for $\mathcal{Q}_k^{(\kappa)} \triangleq I_2\otimes\left(\bar{\mathcal{H}}_k^T(\theta^{(\kappa)})C_k^{(\kappa)}\bar{\mathcal{H}}_k(\theta^{(\kappa)})\right)$.

Thus, we have

$$\begin{aligned}\sum_{k=1}^{K}\gamma_k^{(\kappa)}\tilde{r}_k^{(\kappa)}(\mathbf{w}) &= \sum_{k=1}^{K}\gamma_k^{(\kappa)}a_k^{(\kappa)}\\ &\quad +2\sum_{k=1}^{K}\langle\gamma_k^{(\kappa)}\mathsf{vec}((B_k^{(\kappa)})^T),\mathbf{v}_k\rangle\\ &\quad +\sum_{k=1}^{K}\sum_{j=1}^{K}\mathbf{v}_j^T(\gamma_k^{(\kappa)}\mathcal{Q}_k^{(\kappa)})\mathbf{v}_j\\ &= \sum_{k=1}^{K}\gamma_k^{(\kappa)}a_k^{(\kappa)} + 2\sum_{k=1}^{K}\langle\gamma_k^{(\kappa)}\mathsf{vec}((B_k^{(\kappa)})^T),\mathbf{v}_k\rangle\\ &\quad +\sum_{k=1}^{K}\mathbf{v}_k^T\left(\sum_{j=1}^{K}\gamma_j^{(\kappa)}\mathcal{Q}_j^{(\kappa)}\right)\mathbf{v}_k.\end{aligned} \tag{51}$$

We solve the following convex problem at the κ-th iteration to generate $v^{(\kappa+1)}$:

$$\max_{\mathbf{w}} \sum_{k=1}^{K}\gamma_k^{(\kappa)}\tilde{r}_k^{(\kappa)}(\mathbf{w}) \quad \text{s.t.} \quad (44), \tag{52}$$

which similarly to (16) gives

$$\tilde{F}^{(\kappa)}(v^{(\kappa+1)},\theta^{(\kappa)}) > \tilde{F}^{(\kappa)}(v^{(\kappa)},\theta^{(\kappa)}) \tag{53}$$

as far as $v^{(\kappa+1)} \neq v^{(\kappa)}$.

Like (16), the problem (52) admits the following closed-form solution

$$v_k^{(\kappa+1)} = \begin{cases} \left(\sum_{j=1}^K \gamma_j^{(\kappa)} \mathcal{Q}_j^{(\kappa)}\right)^{-1} \gamma_k^{(\kappa)} \mathsf{vec}((B_k^{(\kappa)})^T) \\ \text{if } \sum_{k=1}^K || \left(\sum_{j=1}^K \gamma_j^{(\kappa)} \mathcal{Q}_j^{(\kappa)}\right)^{-1} \\ \gamma_k^{(\kappa)} \mathsf{vec}((B_k^{(\kappa)})^T)||^2 \leq 2P \\ \left(\sum_{j=1}^K \gamma_j^{(\kappa)} \mathcal{Q}_j^{(\kappa)} + \mu I_M\right)^{-1} \gamma_k^{(\kappa)} \mathsf{vec}((B_k^{(\kappa)})^T) \\ \text{otherwise,} \end{cases} \tag{54}$$

where $\mu > 0$ is found by bisection such that $\sum_{k=1}^K ||\left(\sum_{j=1}^K \gamma_j^{(\kappa)} \mathcal{Q}_j^{(\kappa)} + \mu I_M\right)^{-1} \gamma_k^{(\kappa)} \mathsf{vec}((B_k^{(\kappa)})^T)||^2 = 2P$.

By reconstructing $v_j^{i\ell,(\kappa+1)}$, $i = 1,2$ and $\ell = 1,2$, from $v_j^{(\kappa+1)}$ we use (42) to determine $w_{1,j}^{(\kappa+1)}$ and $w_{2,j}^{(\kappa+1)}$:

$$\begin{aligned} &\begin{bmatrix} \Re\{w_{1,j}^{(\kappa+1)}\} & \Im\{w_{1,j}^{(\kappa+1)}\} \\ \Re\{w_{1,j}^{(\kappa+1)}\} & \Im\{w_{1,j}^{(\kappa+1)}\} \end{bmatrix} \\ &= \frac{1}{2} \begin{bmatrix} v_j^{11,(\kappa+1)} + v_j^{22,(\kappa+1)} & v_j^{21,(\kappa+1)} - v_j^{12,(\kappa+1)} \\ v_j^{11,(\kappa+1)} - v_j^{22,(\kappa+1)} & v_j^{21,(\kappa+1)} + v_j^{12,(\kappa+1)} \end{bmatrix}, \end{aligned} \tag{55}$$

which results in (48).

B. Programmable Reflecting Elements' Descent Iteration

We seek $\theta^{(\kappa+1)}$ such that

$$F^{(\kappa)}(w^{(\kappa+1)}, \theta^{(\kappa+1)}) > F^{(\kappa)}(w^{(\kappa+1)}, \theta^{(\kappa)}). \tag{56}$$

By using the inequality (14) for $\mathbf{V} = \Lambda_k(\boldsymbol{\theta}) W_k^{(\kappa+1)}$, $\mathbf{Y} = \sum_{j \in \mathcal{K} \setminus \{k\}} [\Lambda_k(\boldsymbol{\theta}) W_j^{(\kappa+1)}]^2 + \sigma I_2$, and $\bar{V} = \Lambda_k(\theta^{(\kappa)}) W_k^{(\kappa+1)}$, $\bar{Y} = Y_k^{(\kappa+1)} \triangleq \sum_{j \in \mathcal{K} \setminus \{k\}} [\Lambda_k(\theta^{(\kappa)}) W_j^{(\kappa+1)}]^2 + \sigma I_2 \succeq 0$, we obtain the following concave quadratic lower bounding function approximation of $r_k(w^{(\kappa+1)}, \boldsymbol{\theta})$:

$$\begin{aligned} r_k(w^{(\kappa+1)}, \boldsymbol{\theta}) &\geq \tilde{r}_k^{(\kappa)}(\boldsymbol{\theta}) \\ &\triangleq \tilde{a}_{1k}^{(\kappa)} + 2\Re\{\langle \tilde{B}_k^{(\kappa)} \Lambda_k(\boldsymbol{\theta}) W_k^{(\kappa+1)} \rangle\} \\ &\quad - \langle \tilde{C}_k^{(\kappa)}, \sum_{j \in \mathcal{K}} [\Lambda_k(\boldsymbol{\theta}) W_j^{(\kappa+1)}]^2 \rangle \\ &= \tilde{a}_{1k}^{(\kappa)} + 2\Re\{\langle \tilde{B}_k^{(\kappa)} \Lambda_k(\boldsymbol{\theta}) W_k^{(\kappa+1)} \rangle\} \\ &\quad - \langle \tilde{C}_k^{(\kappa)}, \Lambda_k(\boldsymbol{\theta}) \mathcal{W}_k^{(\kappa+1)} (\Lambda_k(\boldsymbol{\theta}))^H \rangle, \end{aligned} \tag{57}$$

with $\tilde{a}_{1k}^{(\kappa)} \triangleq r_k(w^{(\kappa+1)}, \theta^{(\kappa)}) - \langle [\Lambda_k(\theta^{(\kappa)}) W_k^{(\kappa+1)}]^2 (Y_k^{(\kappa+1)})^{-1} \rangle - \sigma \langle \tilde{C}_k^{(\kappa)} \rangle$, $\tilde{B}_k^{(\kappa)} \triangleq (W_k^{(\kappa+1)})^H (\Lambda_k(\theta^{(\kappa)}))^H (Y_k^{(\kappa+1)})^{-1} \in \mathbb{C}^{2\times 2}$, $0 \prec \tilde{C}_k^{(\kappa)} \triangleq (Y_k^{(\kappa+1)})^{-1} - \left(Y_k^{(\kappa+1)} + [\Lambda_k(\theta^{(\kappa)}) W_k^{(\kappa+1)}]^2\right)^{-1} \in \mathbb{C}^{2\times 2}$, and $0 \prec \mathcal{W}_k^{(\kappa+1)} \triangleq \sum_{j \in \mathcal{K}} [W_j^{(\kappa+1)}]^2$.

For

$$\mathcal{H}_{\text{B-k}} \triangleq \begin{bmatrix} \tilde{h}_{\text{B-k}} & 0_{1\times M} \\ 0_{1\times M} & \tilde{h}^*_{\text{B-k}} \end{bmatrix},$$

we can write

$$\begin{aligned} \Lambda_k(\boldsymbol{\theta}) &= \mathcal{H}_{\text{B-k}} \\ &\quad + \begin{bmatrix} \tilde{h}_{\text{BR-k}} \mathsf{diag}(e^{\jmath\boldsymbol{\theta}}) H_{\text{B-R}} & 0_{1\times M} \\ 0_{1\times M} & \tilde{h}^*_{\text{R-k}} \mathsf{diag}(e^{-\jmath\boldsymbol{\theta}}) H^*_{\text{B-R}} \end{bmatrix} \\ &= \mathcal{H}_{\text{B-k}} + \sum_{n=1}^N \left[\begin{bmatrix} \tilde{h}_{\text{BR-k}} \Psi_n H_{\text{B-R}} & 0_{1\times M} \\ 0_{1\times M} & 0_{1\times M} \end{bmatrix} e^{\jmath\theta_n} \right. \\ &\quad \left. + \begin{bmatrix} 0_{1\times M} & 0_{1\times M} \\ 0_{1\times M} & \tilde{h}^*_{\text{R-k}} \Psi_n H^*_{\text{B-R}} \end{bmatrix} e^{-\jmath\theta_n} \right] \\ &= \mathcal{H}_{\text{B-k}} + \sum_{n=1}^N \left[\Gamma_n e^{\jmath\theta_n} + \Xi_n e^{-\jmath\theta_n} \right], \end{aligned} \tag{58}$$

with

$$\begin{aligned} \Gamma_n &\triangleq \begin{bmatrix} \tilde{h}_{\text{BR-k}} \Psi_n H_{\text{B-R}} & 0_{1\times M} \\ 0_{1\times M} & 0_{1\times M} \end{bmatrix}, n = 1, \ldots, N, \\ \Xi_n &\triangleq \begin{bmatrix} 0_{1\times M} & 0_{1\times M} \\ 0_{1\times M} & \tilde{h}^*_{\text{R-k}} \Psi_n H^*_{\text{B-R}} \end{bmatrix}, n = 1, \ldots, N. \end{aligned} \tag{59}$$

By using the identity

$$\Re\{ab^*\} = \Re\{a^* b\} \quad \forall\, a \in \mathbb{C}, b \in \mathbb{C}, \tag{60}$$

we arrive at:

$$\begin{aligned} &\Re\{\langle \tilde{B}_k^{(\kappa)} \Lambda_k(\boldsymbol{\theta}) W_k^{(\kappa+1)} \rangle\} \\ &\quad = \tilde{a}_{2k}^{(\kappa)} + \Re\{\sum_{n=1}^N (\hat{b}_{1k}^{(\kappa)}(n) e^{\jmath\theta_n} + \hat{b}_{2k}^{(\kappa)}(n) e^{-\jmath\theta_n})\} \\ &\quad = \tilde{a}_{2k}^{(\kappa)} + \Re\{\sum_{n=1}^N \tilde{b}_{2k}^{(\kappa)}(n) e^{\jmath\theta_n}\}, \end{aligned} \tag{61}$$

for $\tilde{a}_{2k}^{(\kappa)} \triangleq \Re\{\langle \tilde{B}_k^{(\kappa)} \mathcal{H}_{\text{B-k}} W_k^{(\kappa+1)} \rangle\}$, $\hat{b}_{1k}^{(\kappa)}(n) \triangleq \langle \tilde{B}_k^{(\kappa)} \Gamma_n W_k^{(\kappa+1)} \rangle$, $\hat{b}_{2k}^{(\kappa)}(n) \triangleq \langle \tilde{B}_k^{(\kappa)} \Xi_n W_k^{(\kappa+1)} \rangle$, and $\tilde{b}_{2k}^{(\kappa)}(n) = \hat{b}_{1k}^{(\kappa)}(n) + (\hat{b}_{2k}^{(\kappa)})^*(n)$, $n = 1, \ldots, N$.

Furthermore, we have (62), shown at the bottom of the next page, where $\tilde{a}_{3k}^{(\kappa)} \triangleq \langle \tilde{C}_k^{(\kappa)}, \mathcal{H}_{\text{B-k}} \mathcal{W}_k^{(\kappa+1)} \mathcal{H}^H_{\text{B-k}} \rangle$, $\tilde{b}_{3k}^{(\kappa)}(n) \triangleq \langle \tilde{C}_k^{(\kappa)}, \mathcal{H}_{\text{B-k}} \mathcal{W}_k^{(\kappa+1)} \Gamma_n^H \rangle^* + \langle \tilde{C}_k^{(\kappa)}, \mathcal{H}_{\text{B-k}} \mathcal{W}_k^{(\kappa+1)} \Xi_n^H \rangle$, $\mathcal{Q}_{11,k}^{(\kappa)}(n,m) = \langle \tilde{C}_k^{(\kappa)}, \Xi_n \mathcal{W}_k^{(\kappa+1)} \Xi_m^H \rangle$, $\mathcal{Q}_{22,k}^{(\kappa)}(n,m) = \langle \tilde{C}_k^{(\kappa)}, \Gamma_m \mathcal{W}_k^{(\kappa+1)} \Gamma_n^H \rangle$, $\mathcal{Q}_{12,k}^{(\kappa)}(n,m) = \langle \tilde{C}_k^{(\kappa)}, \Gamma_n \mathcal{W}_k^{(\kappa+1)} \Xi_m^H \rangle$, $n = 1, \ldots, N$; $m = 1, \ldots, N$.

Let us define

$$\begin{aligned} \mathcal{Q}_{22,k}^{(\kappa)} + \mathcal{Q}_{11,k}^{(\kappa)} &= \mathcal{Q}_{2,k}^{R,(\kappa)} + \jmath \mathcal{Q}_{2,k}^{I,(\kappa)}, \\ &\qquad \mathcal{Q}_{2,k}^{R,(\kappa)} \in \mathbb{R}^{N\times N}, \mathcal{Q}_{2,k}^{I,(\kappa)} \in \mathbb{R}^{N\times N}, \end{aligned}$$

where the matrix $\mathcal{Q}_{2,k}^{R,(\kappa)}$ is symmetric, while the matrix $\mathcal{Q}_{2,k}^{I,(\kappa)}$ is skew-symmetric because the matrix $\mathcal{Q}_{22,k}^{(\kappa)} + \mathcal{Q}_{11,k}^{(\kappa)}$ is Hermitian symmetric, and

$$\mathcal{Q}_{12,k}^{(\kappa)} = \mathcal{Q}_{1,k}^{R,(\kappa)} + \jmath \mathcal{Q}_{1,k}^{I,(\kappa)}, \mathcal{Q}_{1,k}^{R,(\kappa)} \in \mathbb{R}^{N\times N}, \mathcal{Q}_{1,k}^{I,(\kappa)} \in \mathbb{R}^{N\times N}.$$

Upon recalling that $e^{\jmath\boldsymbol{\theta}} = \cos\boldsymbol{\theta} + \jmath \sin\boldsymbol{\theta}$, we have (63) and (64), shown at the bottom of the next page, whose proof is given in the Appendix.

Therefore, we have (65), shown at the bottom of the next page, for $\mathcal{Q}_{k,R}^{(\kappa)} \triangleq \mathcal{Q}_{2,k}^{R,(\kappa)} + \mathcal{Q}_{1,k}^{R,(\kappa)} + (\mathcal{Q}_{1,k}^{R,(\kappa)})^T$, $\mathcal{Q}_{k,C}^{(\kappa)} \triangleq -\mathcal{Q}_{2,k}^{I,(\kappa)} - \mathcal{Q}_{1,k}^{I,(\kappa)} - (\mathcal{Q}_{1,k}^{I,(\kappa)})^T$, $\mathcal{Q}_{k,I}^{(\kappa)} \triangleq \mathcal{Q}_{2,k}^{R,(\kappa)} - \mathcal{Q}_{1,k}^{R,(\kappa)} - (\mathcal{Q}_{1,k}^{R,(\kappa)})^T$.

Combining (57), (61), (62), and (65) yields

$$\gamma_k^{(\kappa)}\tilde{r}^{(\kappa)}(w^{(\kappa+1)},\boldsymbol{\theta}) = \tilde{a}_k^{(\kappa)} + 2\Re\{\sum_{n=1}^{N}\tilde{b}_k^{(\kappa)}(n)e^{\jmath\theta_n}\} - \begin{bmatrix}\cos\boldsymbol{\theta}\\ \sin\boldsymbol{\theta}\end{bmatrix}^T \mathcal{Q}_k^{(\kappa)}\begin{bmatrix}\cos\boldsymbol{\theta}\\ \sin\boldsymbol{\theta}\end{bmatrix} \quad (66)$$

with $\tilde{a}_k^{(\kappa)} = \gamma_k^{(\kappa)}\left(\tilde{a}_{1k}^{(\kappa)} + 2\tilde{a}_{2k}^{(\kappa)} - \tilde{a}_{3k}^{(\kappa)}\right)$, $\tilde{b}_k^{(\kappa)}(n) = \gamma_k^{(\kappa)}\left(\tilde{b}_{2k}^{(\kappa)}(n) - \tilde{b}_{3k}^{(\kappa)}(n)\right)$, $n = 1,\dots,N$, $\mathcal{Q}_k^{(\kappa)} = \gamma_k^{(\kappa)}\begin{bmatrix}\mathcal{Q}_{k,R}^{(\kappa)} & \mathcal{Q}_{k,C}^{(\kappa)}\\ (\mathcal{Q}_{k,C}^{(\kappa)})^T & \mathcal{Q}_{k,I}^{(\kappa)}\end{bmatrix}$.

Therefore, we have:

$$F^{(\kappa)}(w^{(\kappa+1)},\boldsymbol{\theta},\gamma^{(\kappa)}) \geq F_c^{(\kappa)}(\boldsymbol{\theta}) \triangleq \tilde{a}^{(\kappa)} + 2\Re\{\sum_{n=1}^{N}\tilde{b}^{(\kappa)}(n)e^{\jmath\theta_n}\} - \begin{bmatrix}\cos\boldsymbol{\theta}\\ \sin\boldsymbol{\theta}\end{bmatrix}^T \mathcal{Q}^{(\kappa)}\begin{bmatrix}\cos\boldsymbol{\theta}\\ \sin\boldsymbol{\theta}\end{bmatrix} \quad (67)$$

for $\tilde{a}^{(\kappa)} = \sum_{k=1}^K \tilde{a}_k^{(\kappa)}$, $\tilde{b}^{(\kappa)}(n) = \sum_{k=1}^K \tilde{b}_k^{(\kappa)}(n), n = 1,\dots,N$, and $\mathcal{Q}^{(\kappa)} = \sum_{k=1}^K \mathcal{Q}_k^{(\kappa)} = \begin{bmatrix}\mathcal{Q}_R^{(\kappa)} & \mathcal{Q}_C^{(\kappa)}\\ (\mathcal{Q}_C^{(\kappa)})^T & \mathcal{Q}_I^{(\kappa)}\end{bmatrix}$, with $\mathcal{Q}_R^{(\kappa)} = \sum_{k=1}^K \mathcal{Q}_{k,R}^{(\kappa)}, \mathcal{Q}_C^{(\kappa)} = \sum_{k=1}^K \mathcal{Q}_{k,C}^{(\kappa)}, \mathcal{Q}_I^{(\kappa)} = \sum_{k=1}^K \mathcal{Q}_{k,I}^{(\kappa)}$.

Furthermore, we have (68), shown at the bottom of the next page.

Now, using the formula

$$\alpha^{R,(\kappa)}(n)\cos\boldsymbol{\theta}_n + \alpha^{I,(\kappa)}(n)\sin\boldsymbol{\theta}_n = \Re\{\beta(n)e^{\jmath\boldsymbol{\theta}_n}\}$$

for $\beta(n) = \sqrt{(\alpha^{R,(\kappa)}(n))^2 + (\alpha^{I,(\kappa)}(n))^2}e^{-\jmath\gamma(n)}$, where $\gamma(n)$ is such that $[\cos\gamma(n), \sin\gamma(n)] = [\alpha^{R,(\kappa)}(n), \alpha^{I,(\kappa)}(n)]/\sqrt{[\alpha^{R,(\kappa)}(n)]^2 + [\alpha^{I,(\kappa)}(n)]^2}$, we can rewrite (68) by

$$\tilde{F}_c^{(\kappa)}(\boldsymbol{\theta}) = \tilde{\tilde{a}}^{(\kappa)} + 2\Re\{\sum_{n=1}^{N}\tilde{b}^{(\kappa)}(n)e^{\jmath\theta_n}\rangle\}$$

$$\begin{aligned}
\langle\tilde{C}_k^{(\kappa)}, \Lambda_k(\boldsymbol{\theta})\mathcal{W}_k^{(\kappa+1)}\Lambda_k^H(\boldsymbol{\theta})\rangle &= \langle\tilde{C}_k^{(\kappa)}, \left[\sum_{n=1}^N\left(\Gamma_n e^{\jmath\theta_n} + \Xi_n e^{-\jmath e^{\jmath\theta_n}}\right) + \mathcal{H}_{\text{B-k}}\right]\mathcal{W}_k^{(\kappa+1)}\left[\sum_{n=1}^N\left(\Gamma_n^H e^{-\jmath\theta_n} + \Xi_n^H e^{\jmath\theta_n}\right) + \mathcal{H}_{\text{B-k}}^H\right]\rangle\\
&= \langle\tilde{C}_k^{(\kappa)}, \mathcal{H}_{\text{B-k}}\mathcal{W}_k^{(\kappa+1)}\mathcal{H}_{\text{B-k}}^H\rangle + 2\Re\{\langle\tilde{C}_k^{(\kappa)}, \mathcal{H}_{\text{B-k}}\mathcal{W}_k^{(\kappa+1)}\sum_{n=1}^N\left(\Gamma_n^H e^{-\jmath\theta_n} + \Xi_n^H e^{\jmath\theta_n}\right)\}\\
&\quad + \langle\tilde{C}_k^{(\kappa)}, \left[\sum_{n=1}^N\left(\Gamma_n e^{\jmath\theta_n} + \Xi_n e^{-\jmath\theta_n}\right)\right]\mathcal{W}_k^{(\kappa+1)}\left[\sum_{n=1}^N\left(\Gamma_n^H e^{-\jmath\theta_n} + \Xi_n^H e^{\jmath\theta_n}\right)\right]\rangle\\
&= \langle\tilde{C}_k^{(\kappa)}, \mathcal{H}_{\text{B-k}}\mathcal{W}_k^{(\kappa+1)}\mathcal{H}_{\text{B-k}}^H\rangle\\
&\quad + 2\Re\{\sum_{n=1}^N\left(\langle\tilde{C}_k^{(\kappa)}, \mathcal{H}_{\text{B-k}}\mathcal{W}_k^{(\kappa+1)}\Gamma_n^H\rangle^* + \langle\tilde{C}_k^{(\kappa)}, \mathcal{H}_{\text{B-k}}\mathcal{W}_k^{(\kappa+1)}\Xi_n^H\rangle\right)e^{\jmath\theta_n}\}\\
&\quad + \sum_{n=1}^N\sum_{m=1}^N\langle\tilde{C}_k^{(\kappa)}, \Gamma_n\mathcal{W}_k^{(\kappa+1)}\Gamma_m^H\rangle e^{\jmath\theta_n}e^{-\jmath\theta_m} + \sum_{n=1}^N\sum_{m=1}^N\langle\tilde{C}_k^{(\kappa)}, \Gamma_n\mathcal{W}_k^{(\kappa+1)}\Xi_m^H\rangle e^{\jmath\theta_n}e^{-\jmath\theta_m}\\
&\quad + \sum_{n=1}^N\sum_{m=1}^N\langle\tilde{C}_k^{(\kappa)}, \Xi_n\mathcal{W}_k^{(\kappa+1)}\Gamma_m^H\rangle e^{-\jmath\theta_n}e^{-\jmath\theta_m} + \sum_{n=1}^N\sum_{m=1}^N\langle\tilde{C}_k^{(\kappa)}, \Xi_n\mathcal{W}_k^{(\kappa+1)}\Xi_m^H\rangle e^{-\jmath\theta_n}e^{-\jmath\theta_m}\\
&= \tilde{a}_{3k}^{(\kappa)} + 2\Re\{\sum_{n=1}^N\tilde{b}_{3k}^{(\kappa)}(n)e^{\jmath\theta_n}\rangle\} + (e^{\jmath\boldsymbol{\theta}})^H\mathcal{Q}_{22,k}^{(\kappa)}e^{\jmath\boldsymbol{\theta}} + (e^{\jmath\boldsymbol{\theta}})^T\mathcal{Q}_{12,k}^{(\kappa)}e^{\jmath\boldsymbol{\theta}} + (e^{\jmath\boldsymbol{\theta}})^H(\mathcal{Q}_{12,k}^{(\kappa)})^*e^{-\jmath\boldsymbol{\theta}}\\
&\quad + (e^{\jmath\boldsymbol{\theta}})^H\mathcal{Q}_{11,k}^{(\kappa)}e^{\jmath\boldsymbol{\theta}},
\end{aligned} \quad (62)$$

$$(e^{\jmath\boldsymbol{\theta}})^H(\mathcal{Q}_{22,k}^{(\kappa)} + \mathcal{Q}_{11,k}^{(\kappa)})e^{\jmath\boldsymbol{\theta}} = \begin{bmatrix}\cos\boldsymbol{\theta}\\ \sin\boldsymbol{\theta}\end{bmatrix}^T\begin{bmatrix}\mathcal{Q}_{2,k}^{R,(\kappa)} & -\mathcal{Q}_{2,k}^{I,(\kappa)}\\ \mathcal{Q}_{2,k}^{I,(\kappa)} & \mathcal{Q}_{2,k}^{R,(\kappa)}\end{bmatrix}\begin{bmatrix}\cos\boldsymbol{\theta}\\ \sin\boldsymbol{\theta}\end{bmatrix}, \quad (63)$$

$$\begin{aligned}(e^{\jmath\boldsymbol{\theta}})^T\mathcal{Q}_{12,k}^{(\kappa)}e^{\jmath\boldsymbol{\theta}} + (e^{\jmath\boldsymbol{\theta}})^H(\mathcal{Q}_{12,k}^{(\kappa)})^*e^{-\jmath\boldsymbol{\theta}} &= \begin{bmatrix}\cos\boldsymbol{\theta}\\ \sin\boldsymbol{\theta}\end{bmatrix}^T\\
&\quad\begin{bmatrix}\mathcal{Q}_{1,k}^{R,(\kappa)} + (\mathcal{Q}_{1,k}^{R,(\kappa)})^T & -\mathcal{Q}_{1,k}^{I,(\kappa)} - (\mathcal{Q}_{1,k}^{I,(\kappa)})^T\\ -\mathcal{Q}_{1,k}^{I,(\kappa)} - (\mathcal{Q}_{1,k}^{I,(\kappa)})^T & -\mathcal{Q}_{1,k}^{R,(\kappa)} - (\mathcal{Q}_{1,k}^{R,(\kappa)})^T\end{bmatrix}\begin{bmatrix}\cos\boldsymbol{\theta}\\ \sin\boldsymbol{\theta}\end{bmatrix},\end{aligned} \quad (64)$$

$$(e^{\jmath\boldsymbol{\theta}})^H(\mathcal{Q}_{22,k}^{(\kappa)} + \mathcal{Q}_{11,k}^{(\kappa)})e^{\jmath\boldsymbol{\theta}} + (e^{\jmath\boldsymbol{\theta}})^T\mathcal{Q}_{12,k}^{(\kappa)}e^{\jmath\boldsymbol{\theta}} + (e^{\jmath\boldsymbol{\theta}})^H(\mathcal{Q}_{12,k}^{(\kappa)})^*e^{-\jmath\boldsymbol{\theta}} = \begin{bmatrix}\cos\boldsymbol{\theta}\\ \sin\boldsymbol{\theta}\end{bmatrix}^T\begin{bmatrix}\mathcal{Q}_{k,R}^{(\kappa)} & \mathcal{Q}_{k,C}^{(\kappa)}\\ (\mathcal{Q}_{k,C}^{(\kappa)})^T & \mathcal{Q}_{k,I}^{(\kappa)}\end{bmatrix}\begin{bmatrix}\cos\boldsymbol{\theta}\\ \sin\boldsymbol{\theta}\end{bmatrix} \quad (65)$$

$$-2\sum_{n=1}^{N}\Re\{\beta(n)e^{\jmath\boldsymbol{\theta}_n}\}$$
$$=\tilde{\tilde{a}}^{(\kappa)}+2\sum_{n=1}^{N}\Re\{\left(\tilde{b}^{(\kappa)}(n)-\beta(n)\right)e^{\jmath\boldsymbol{\theta}_n}\}. \quad (69)$$

Accordingly, we solve the following convex problem at the κ-th iteration to generate $\theta^{(\kappa+1)}$:

$$\max_{\boldsymbol{\theta}}\ \tilde{F}_c^{(\kappa)}(\boldsymbol{\theta}). \quad (70)$$

Like (29), its optimal solution is given in closed-form by

$$\theta_n^{(\kappa+1)}=-\angle\left(\tilde{b}^{(\kappa)}(n)-\beta(n)\right), n=1,\ldots,N. \quad (71)$$

It follows from (68) that $F^{(\kappa)}(w^{(\kappa+1)},\theta^{(\kappa+1)}) \geq F_c^{(\kappa)}(\theta^{(\kappa+1)}) \geq \tilde{F}_c^{(\kappa)}(\theta^{(\kappa+1)}) > \tilde{F}_c^{(\kappa)}(\theta^{(\kappa)}) = F_c^{(\kappa)}(\theta^{(\kappa)}) = F^{(\kappa)}(w^{(\kappa+1)},\theta^{(\kappa)})$, confirming (56), so $\theta^{(\kappa+1)}$ is a better feasible point than $\theta^{(\kappa)}$.

C. Improper Gaussian Signaling Geometric Mean Rate Optimization

All other exiting algorithms, which solve convex problems and iteratively at a high complexity are very sensitive to the problem sizes. However, our algorithms iterate using closed-form expressions, hence their complexity is low. Algorithm 2 provides the pseudo-code for the proposed computational procedure for the solution of (36).

Algorithm 2 IGS GM Descent Algorithm

1: **Initialization:** Set $\kappa=0$. Randomly generate $(\theta^{(0)},w^{(0)})$ satisfying the constraint (35b) and then define $\gamma^{(0)}$ by (12).
2: **Repeat until convergence of the objective in** (36)**:** Generate $w^{(\kappa+1)}$ by (54)- (55) and $\theta^{(\kappa+1)}$ by (71). Reset $\kappa\leftarrow\kappa+1$.
3: **Output** $(w^{(\kappa)},\theta^{(\kappa)})$ and the rates $r_k(w^{(\kappa)},\theta^{(\kappa)})$, $k=1,\ldots,K$ with their GM $(\prod_{k=1}^{K}r_k(w^{(\kappa)},\theta^{(\kappa)}))^{1/K}$.

IV. Numerical Examples

This section evaluates the efficiency of the proposed algorithms by numerical examples. Table II provides the numerical values of the main parameters taken from [21], [34] for numerical characterization. Furthermore, the elements of the BS-to-RIS LoS channel matrix are generated by $[H_{\text{B-R}}]_{n,m}=e^{j\pi\left((n-1)\sin\bar{\theta}_n\sin\bar{\phi}_n+(m-1)\sin e^{\jmath\theta_n}\sin\phi_n\right)}$, where $e^{\jmath\theta_n}$ and ϕ_n are uniformly distributed as $e^{\jmath\theta_n}\sim\mathcal{U}(0,\pi)$ and $\phi_n\sim\mathcal{U}(0,2\pi)$, respectively, and $\bar{\theta}_n=\pi-\theta_n$ and $\bar{\phi}_n=\pi+\phi_n$ [21]. The normalized small-scale fading channel $h_{\text{B-k}}$ spanning from the BS to UE k follows the classic Rayleigh distribution, while the small-scale fading channel gain $h_{\text{R-k}}$ of the RIS to UE k obeys Rician distribution with a K-factor of 3. The spatial correlation matrix is given by $[\mathbf{R}_{\text{R-k}}]_{n,n'}=e^{j\pi(n-n')\sin\tilde{\phi}_k\sin\tilde{\theta}_k}$, where $\tilde{\phi}_k$ and $\tilde{\theta}$ are the azimuth and elevation angle for UE k, respectively. Unless otherwise stated, $P=20$dBm and $N=100$ are used. The results are multiplied by $\log_2\ e$ to convert the unit nats/sec into the unit bps/Hz. The convergence tolerance of the proposed algorithms is set to 10^{-3}. For computational stability, $\gamma_k^{(\kappa)}$ in (12) is scaled as

$$\gamma_k^{(\kappa)}\rightarrow\frac{\gamma_k^{(\kappa)}}{\min_{j=1,\ldots,K}\gamma_j^{(\kappa)}}, k=1,\ldots,K. \quad (72)$$

For the setup of Fig. 1 the BS and the RIS are deployed at the coordinates of $(40,0,25)$ and $(0,60,40)$ in the three-dimensional (3D) space, while $K=10$ UEs are randomly placed in a $(120m\times120\ m)$ area right of the BS and RIS. In what follows, we refer to SR-PGS and SR-IGS

$$\begin{aligned}
F_c^{(\kappa)}(\boldsymbol{\theta}) &= \tilde{a}^{(\kappa)}+2\Re\{\sum_{n=1}^{N}\tilde{b}^{(\kappa)}(n)e^{\jmath\theta_n}\rangle\}-\begin{bmatrix}\cos\boldsymbol{\theta}\\ \sin\boldsymbol{\theta}\end{bmatrix}^T\left(\mathcal{Q}^{(\kappa)}-\lambda_{\max}(\mathcal{Q}^{(\kappa)})I_{2N}\right)\begin{bmatrix}\cos\boldsymbol{\theta}\\ \sin\boldsymbol{\theta}\end{bmatrix}\\
&\quad-\lambda_{\max}(\mathcal{Q}^{(\kappa)})N\\
&\geq \tilde{a}^{(\kappa)}+2\Re\{\sum_{n=1}^{N}\tilde{b}^{(\kappa)}(n)e^{\jmath\theta_n}\rangle\}-2\begin{bmatrix}\cos\theta^{(\kappa)}\\ \sin\theta^{(\kappa)}\end{bmatrix}^T\left(\mathcal{Q}^{(\kappa)}-\lambda_{\max}(\mathcal{Q}^{(\kappa)})I_{2N}\right)\begin{bmatrix}\cos\boldsymbol{\theta}\\ \sin\boldsymbol{\theta}\end{bmatrix}\\
&\quad+\begin{bmatrix}\cos\theta^{(\kappa)}\\ \sin\theta^{(\kappa)}\end{bmatrix}^T\left(\mathcal{Q}^{(\kappa)}-\lambda_{\max}(\mathcal{Q}^{(\kappa)})I_{2N}\right)\begin{bmatrix}\cos\theta^{(\kappa)}\\ \sin\theta^{(\kappa)}\end{bmatrix}-\lambda_{\max}(\mathcal{Q}^{(\kappa)})N\\
&= \tilde{\tilde{a}}^{(\kappa)}+2\Re\{\sum_{n=1}^{N}\tilde{b}^{(\kappa)}(n)e^{\jmath\theta_n}\rangle\}-2\sum_{n=1}^{N}\left(\alpha^{R,(\kappa)}(n)\cos\boldsymbol{\theta}_n+\alpha^{I,(\kappa)}(n)\sin\boldsymbol{\theta}_n\right)\\
&\triangleq \tilde{F}_c^{(\kappa)}(\boldsymbol{\theta}),
\end{aligned} \quad (68)$$

with

$$\begin{aligned}
\tilde{\tilde{a}}^{(\kappa)} &= \tilde{a}^{(\kappa)}-\begin{bmatrix}\cos\theta^{(\kappa)}\\ \sin\theta^{(\kappa)}\end{bmatrix}^T\mathcal{Q}^{(\kappa)}\begin{bmatrix}\cos\theta^{(\kappa)}\\ \sin\theta^{(\kappa)}\end{bmatrix}-2\lambda_{\max}(\mathcal{Q}^{(\kappa)})N,\\
\alpha^{R,(\kappa)} &= (\theta^{R,(\kappa)})^T\left(\mathcal{Q}_R^{(\kappa)}-\lambda_{\max}(\mathcal{Q}^{(\kappa)})I_N\right)+(\theta^{I,(\kappa)})^T(\mathcal{Q}_C^{(\kappa)})^T\in\mathbb{R}^{1\times N},\\
\alpha^{I,(\kappa)} &= (\theta^{R,(\kappa)})^T(\mathcal{Q}_C^{(\kappa)})+(\theta^{I,(\kappa)})^T\left(\mathcal{Q}_I^{(\kappa)}-\lambda_{\max}(\mathcal{Q}^{(\kappa)})I_N\right)\in\mathbb{R}^{1\times N}.
\end{aligned}$$

TABLE II
MAJOR PARAMETERS SETUP

Parameter	Numerical value
BS-to-RIS path-loss $\beta_{\text{B-R}}$ at the distance $d_{\text{B-R}}$ in (4)	$G_{\text{BS}} + G_{\text{RIS}} - 35.9 - 22\log_{10}(d_{\text{B-R}})$ (in dB)
RIS-to-UE path-loss $\beta_{\text{R-k}}$ at the distance $d_{\text{R-k}}$ in (4)	$G_{\text{RIS}} - 33.05 - 30\log_{10}(d_{\text{R-k}})$ (in dB)
BS-to-UE Path-loss $\beta_{\text{B-k}}$ at the distance $d_{\text{B-k}}$ in (4)	$G_{\text{BS}} - 33.05 - 36.7\log_{10}(d_{\text{B-k}})$ (in dB)
Antenna gain G_{BS} of the BS and G_{RIS} of the RIS elements	5 dBi
Bandwidth	1MHz
Noise power density	-174 dBm/Hz

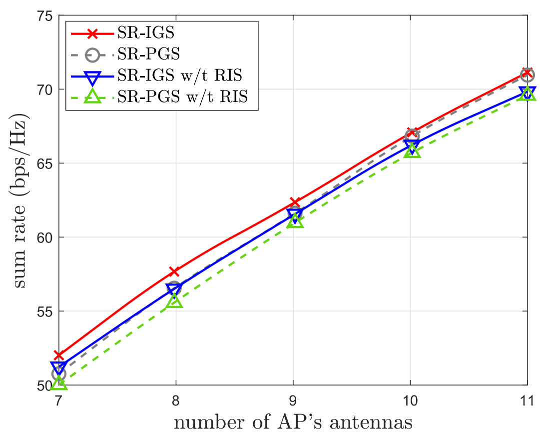

Fig. 2. SR versus the number of antennas M.

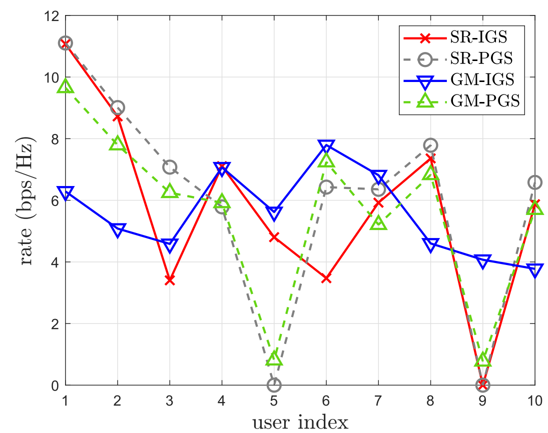

Fig. 3. Rate distribution for $M = 9$.

as the SR under PGS and IGS, which are achieved by iterating (18) and (29), and (54) and (55) with $\gamma_k^{(\kappa)} \equiv 1$. Their stand-alone counter-parts dispensing with the RIS are referred by SR-PGS w/t RIS and SR-IGS w/t RIS, which are achieved by iterating (18) and (54) with $\gamma_k^{(\kappa)} \equiv 1$ in the corresponding stand-alone models. Another pair of counter-parts labelled by SR-PGS-RIS w. random $\boldsymbol{\theta}$ and SR-IGS-RIS w. random $\boldsymbol{\theta}$ represent the SR with the PREs randomly selected, which correspond to iterating (18) and (54) under a fixed $\theta^{(\kappa)} = \bar{\theta}$ with $\gamma_k^{(\kappa)} \equiv 1$. Finally, GM-PGS-RIS and GM-IGS-RIS represent to the achievable GMs under PGS and IGS, which are computed by Algorithm 1 and 2.

Fig. 2 plots the SR performance versus the number M of antennas at the BS. The SR-PGS and SR-IGS are only slightly better than their counter-parts SR-IGS w/t RIS and SR-PGS, because the direct channel $\tilde{h}_{\text{B-k}}$ spanning from the BS to UE k is much stronger than the reflected channel $\tilde{h}_{\text{R-k}}\mathbf{R}_{\text{R-k}}^{1/2}(e^{\jmath\boldsymbol{\theta}})\tilde{H}_{\text{B-R}}$. The performance margin becomes wider with M increased. Furthermore, SR-PGS approaches SR-IGS for $M \geq K$ in Fig. 2.

Next, Fig. 3 portrays a rate distribution pattern for $(M, N, P) = (9, 100, P = 20\text{dBm})$. Observe in the figure that only GM-IGS and GM-PGS are capable of avoiding the assignment of zero rate, hence demonstrating its superiority.

To substantiate this fact, Table III provides the average number of zero-rate users (ZR-UEs) for the optimization schemes considered under different number of antennas M. For SR-IGS and SR-PGS, the number of ZR-UEs increases when M is reduced. SR-PGS results in more ZR-UEs than SR-IGS, while there are no ZR-UEs in GM-IGS and GM-PGS, confirming that both of them are beneficial in providing the adequate rates to all users.

TABLE III
THE AVERAGE NUMBER OF ZR-UES VERSUS M

Number of antennas	SR-IGS	SR-PGS	GM-IGS	GM-PGS
M = 7	0.33	3.13	0	0
M = 8	0.23	2.37	0	0
M = 9	0.17	1.64	0	0
M = 10	0	1.10	0	0
M = 11	0	0.72	0	0

Furthermore, we also examine the resultant ratio of the minimum rate and maximum rate (min-rate/max-rate) and the resultant rate-variance of these schemes versus the number of antennas, M. Fig. 4 shows that both GM-PGS and GM-IGS produce min-rate/max-rates that are substantially higher than that of SR-PGS and SR-IGS. SR-IGS produces higher min-rate/max-rates than SR-PGS does. Fig. 4 also shows the min-rate/max-rate of SR-PGS remains zero for $M < K$ since there are always some ZR-UEs. Furthermore, upon increasing the number of AP antennas, both the min-rate and the max-rate both are improved due to the increased benefit of spatial diversity, but the value of min-rate /max-rate is not necessary a monotonic function of the number of AP antennas. In Fig. 5, the rate variance of SR-PGS is seen to be twice of that by its IGS counter SR-IGS at $M = 7$. The discrepancy becomes narrower upon increasing M and it is closer to zero for $M = 11$. The rate-variances are beneficially reduced by the GM-maximization based schemes GM-IGS and GM-PGS. Both Fig. 4 and Fig. 5 indicate the advantages of IGS over PGS both in terms of SR and GM maximization.

Fig. 6 shows the GM rates. As expected, GM-IGS and GM-PGS produce much better GM rate than that of SR-IGS and SR-PGS. Note that GM-PGS has better GM rates than GM-IGS for $M > K$ due to the well-known capability of PGS to mitigate the multi-user interference, when the number of transmit antennas is higher than the number of users.

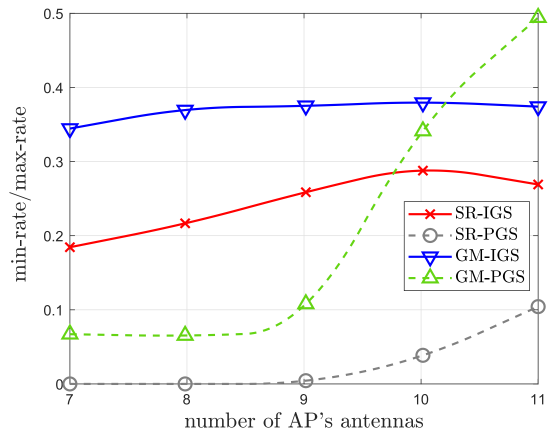

Fig. 4. Min-rate/max-rate versus the number of antennas M.

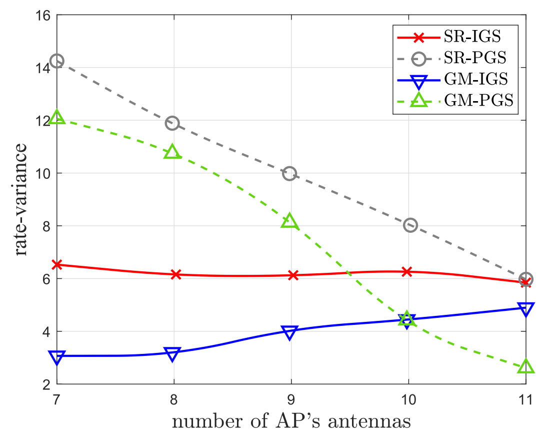

Fig. 5. Rate-variance versus the number of antennas M.

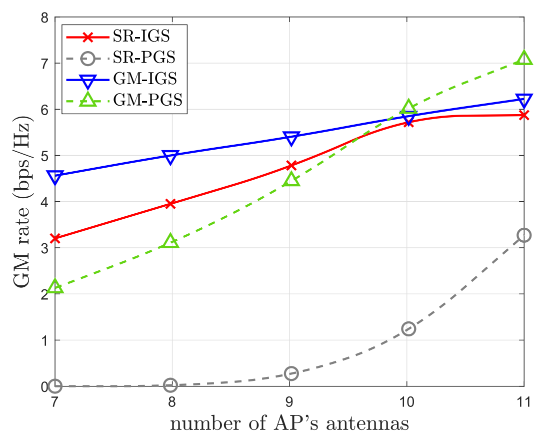

Fig. 6. GM versus the number of antennas M.

We also consider another scenario as illustrated by Fig. 7, where the direct signal path between the BS and users is blocked, i.e. we have $h_{\text{B-k}} \equiv 0$ in (2) and (4). The distances between the BS and users becomes slightly smaller upon deploying the BS at the coordinates $(20, 0, 25)$ and the RIS at the coordinates $(0, 30, 40)$. In this scenario, $K = 10$ UEs are randomly placed in a $(60m \times 60\ m)$ area right of the BS and RIS.

Fig. 8 portrays the SR versus M, where SR-IGS outperforms SR-PGS. Furthermore, both the former and the latter substantially outperform their counter-parts SR-IGS w.

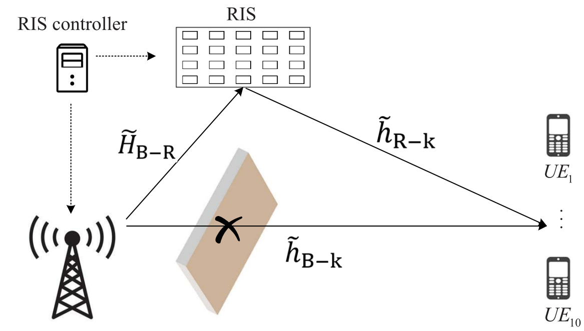

Fig. 7. System model.

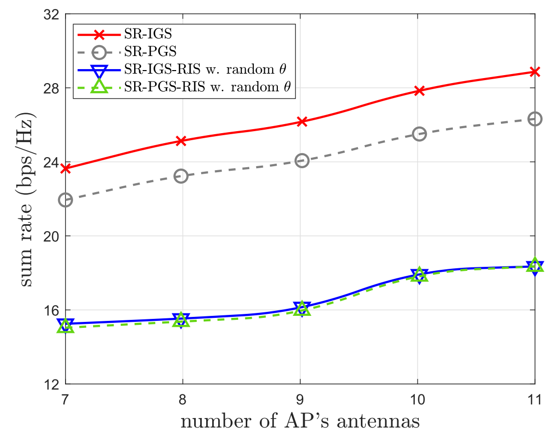

Fig. 8. SR versus the number of antennas M.

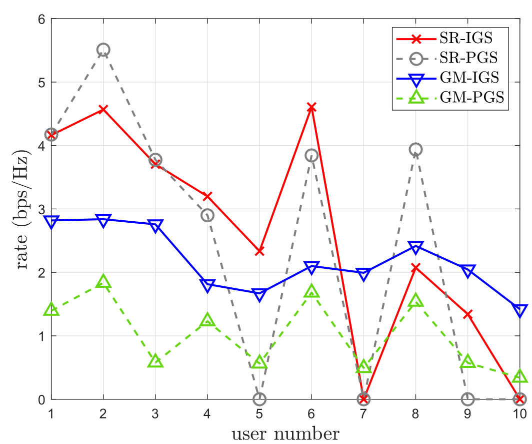

Fig. 9. User rate distribution for $M = 9$.

random θ and SR-PGS w. random θ operating without an RIS.

Similarly to Fig. 3, Fig. 9 shows a typical user rate distribution, where both the GM maximization based GM-IGS and GM-PGS schemes assign more transmit power to the users having worse channel conditions for achieving fair rate distributions.

Table IV shows the average number of ZR-UEs versus M, demonstrating that the number of ZR-UEs for both SR-IGS and SR-PGS is higher than 3, with that of SR-PGS having higher than that of SR-IGS. As expected, there are no ZR-UEs for GM-IGS and GM-PGS.

Fig. 10 and Fig. 11 plot the min-rate/max-rate and rate-variance versus M, respectively. The min-rate/max-rate of SR-IGS and SR-PGS remains zero for the practical range of

TABLE IV

THE AVERAGE NUMBER OF ZR-UEs VERSUS THE NUMBER OF ANTENNAS M

Number of antennas	SR-IGS	SR-PGS	GM-IGS	GM-PGS
M = 7	3.97	5.40	0	0
M = 8	3.63	4.79	0	0
M = 9	3.20	5.61	0	0
M = 10	3.30	4.13	0	0
M = 11	3.11	3.82	0	0

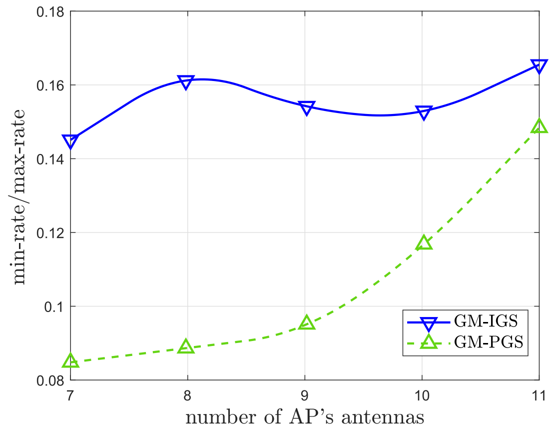

Fig. 10. Min-rate/max-rate versus the number of antennas M.

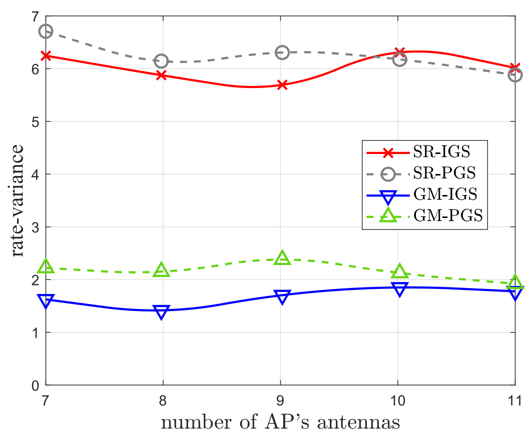

Fig. 11. Rate-variance versus the number of antennas M.

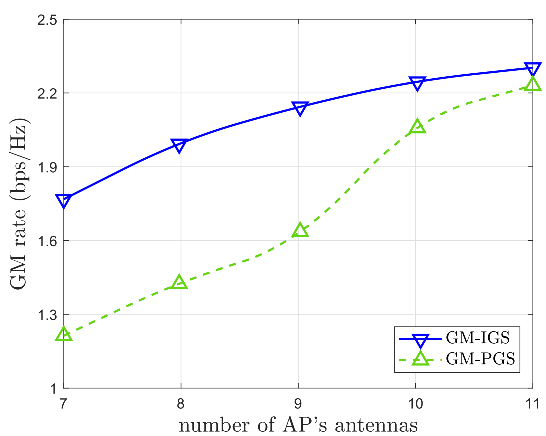

Fig. 12. GM rate versus the number of antennas M.

$M \in \{7, \dots, 11\}$. Furthermore, GM-IGS has a better performance than GM-PGS. Fig. 11 shows that the rate variance is substantially improved by the GM-based maximization, where GM-IGS results in much better rate variance than GM-PGS. The advantage of GM rate maximization based IGS becomes quite convincing.

Finally, Fig. 12 plots the GM rate versus M, which remains zero for both SR-IGS and SR-PGS for $M \in \{7, \dots, 11\}$, because there are ZR-UEs. The performance of GM-PGS gets closer to that of GM-IGS for $M \geq K$. The advantage of rates GM maximization based IGS is well justified in above results.

V. CONCLUSION

In this paper, we have considered the maximization of the geometric mean (GM) of users' rates for the sake of maintaining a uniform quality-of-service for the downlink users of an RIS-aid communication network. The computationally intractable unit modulus constraint imposed on the programmable reflecting coefficients has been eliminated by directly optimizing their argument. The problem of maximizing the users' GM rate has been solved by the proposed alternating descent iterations leading to a closed-form solution for the associated convex problems and thus it is computationally efficient. The numerical examples provided have shown a substantially improved rate-fairness amongst the users. Extension of the GM maximization-based approach to multi-carrier communication is under our current study. Its extension to quantized RIS-aided communication is also interesting and deserves a separate study in our future research.

APPENDIX
PROOF OF (63) AND (64)

Note that

$$\mathcal{Q}_{22,k}^{(\kappa)} + \mathcal{Q}_{11,k}^{(\kappa)} = \mathcal{Q}_{2,k}^{R,(\kappa)} + \jmath \mathcal{Q}_{2,k}^{I,(\kappa)}$$

and $\mathcal{Q}_{2,k}^{R,(\kappa)}$ is symmetric, while $\mathcal{Q}_{2,k}^{I,(\kappa)}$ is anti-symmetric ($\mathcal{Q}_{2,k}^{I,(\kappa)} = -(\mathcal{Q}_{2,k}^{I,(\kappa)})^T$, hence we have $x^T \mathcal{Q}_{2,k}^{I,(\kappa)} x = 0 \ \forall\, x \in \mathbb{R}^N$).

Then the

$$\begin{aligned}
&\text{LHS of (63)} \\
&= (\cos\boldsymbol{\theta} - \jmath \sin\boldsymbol{\theta})^T \left(\mathcal{Q}_{2,k}^{R,(\kappa)} + \jmath \mathcal{Q}_{2,k}^{I,(\kappa)}\right)(\cos\boldsymbol{\theta} + \jmath \sin\boldsymbol{\theta}) \\
&= \Big((\cos\boldsymbol{\theta})^T \mathcal{Q}_{2,k}^{R,(\kappa)} - \jmath(\sin\boldsymbol{\theta})^T \mathcal{Q}_{2,k}^{R,(\kappa)} + \jmath(\cos\boldsymbol{\theta})^T \mathcal{Q}_{2,k}^{I,(\kappa)} \\
&\quad -(\sin\boldsymbol{\theta})^T \mathcal{Q}_{2,k}^{I,(\kappa)}\Big)(\cos\boldsymbol{\theta} + \jmath \sin\boldsymbol{\theta}) \\
&= (\cos\boldsymbol{\theta})^T \mathcal{Q}_{2,k}^{R,(\kappa)} \cos\boldsymbol{\theta} - \jmath(\sin\boldsymbol{\theta})^T \mathcal{Q}_{2,k}^{R,(\kappa)} \cos\boldsymbol{\theta} \\
&\quad + \jmath(\cos\boldsymbol{\theta})^T \mathcal{Q}_{2,k}^{I,(\kappa)} \cos\boldsymbol{\theta} - (\sin\boldsymbol{\theta})^T \mathcal{Q}_{2,k}^{I,(\kappa)} \cos\boldsymbol{\theta} \\
&\quad + \jmath(\cos\boldsymbol{\theta})^T \mathcal{Q}_{2,k}^{R,(\kappa)} \sin\boldsymbol{\theta} + (\sin\boldsymbol{\theta})^T \mathcal{Q}_{2,k}^{R,(\kappa)} \sin\boldsymbol{\theta} \\
&\quad - (\cos\boldsymbol{\theta})^T \mathcal{Q}_{2,k}^{I,(\kappa)} \sin\boldsymbol{\theta} - \jmath(\sin\boldsymbol{\theta})^T \mathcal{Q}_{2,k}^{I,(\kappa)} \sin\boldsymbol{\theta} \\
&= (\cos\boldsymbol{\theta})^T \mathcal{Q}_{2,k}^{R,(\kappa)} \cos\boldsymbol{\theta} - (\sin\boldsymbol{\theta})^T \mathcal{Q}_{2,k}^{I,(\kappa)} \cos\boldsymbol{\theta} \\
&\quad + (\sin\boldsymbol{\theta})^T \mathcal{Q}_{2,k}^{R,(\kappa)} \sin\boldsymbol{\theta} - (\cos\boldsymbol{\theta})^T \mathcal{Q}_{2,k}^{I,(\kappa)} \sin\boldsymbol{\theta} \\
&= \text{RHS of (63)},
\end{aligned}$$

proving (63).

Furthermore,

$$\begin{aligned}
&\text{LHS of (64)} \\
&\quad = 2\Re\{(e^{\jmath\boldsymbol{\theta}})^T \mathcal{Q}_{12,k}^{(\kappa)} e^{\jmath\boldsymbol{\theta}}\}
\end{aligned}$$

$$
\begin{aligned}
&= 2\Re\left\{(\cos\boldsymbol{\theta}+\jmath\sin\boldsymbol{\theta})^T\left(\mathcal{Q}_{1,k}^{R,(\kappa)}+\jmath\mathcal{Q}_{1,k}^{I,(\kappa)}\right)\right.\\
&\quad\left.(\cos\boldsymbol{\theta}+\jmath\sin\boldsymbol{\theta})\right\}\\
&= 2\left((\cos\boldsymbol{\theta})^T\mathcal{Q}_{1,k}^{R,(\kappa)}\cos\boldsymbol{\theta}-(\cos\boldsymbol{\theta})^T\mathcal{Q}_{1,k}^{I,(\kappa)}\sin\boldsymbol{\theta}\right.\\
&\quad\left.-(\sin\boldsymbol{\theta})^T\mathcal{Q}_{1,k}^{R,(\kappa)}\sin\boldsymbol{\theta}-(\sin\boldsymbol{\theta})^T\mathcal{Q}_{1,k}^{I,(\kappa)}\cos\boldsymbol{\theta}\right)\\
&= \text{RHS of (64)},
\end{aligned}
$$

proving (64).

References

[1] H. H. M. Tam, H. D. Tuan, and D. T. Ngo, "Successive convex quadratic programming for quality-of-service management in full-duplex MU-MIMO multicell networks," *IEEE Trans. Commun.*, vol. 64, no. 6, pp. 2340–2353, Jun. 2016.

[2] L. D. Nguyen, H. D. Tuan, T. Q. Duong, H. V. Poor, and L. Hanzo, "Energy-efficient multi-cell massive MIMO subject to minimum user-rate constraints," *IEEE Trans. Commun.*, vol. 69, no. 2, pp. 914–928, Feb. 2021.

[3] T. Yoo and A. Goldsmith, "On the optimality of multiantenna broadcast scheduling using zero-forcing beamforming," *IEEE J. Sel. Areas Commun.*, vol. 24, no. 3, pp. 528–541, Mar. 2006.

[4] L. D. Nguyen, H. D. Tuan, T. Q. Duong, O. A. Dobre, and H. V. Poor, "Downlink beamforming for energy-efficient heterogeneous networks with massive MIMO and small cells," *IEEE Trans. Wireless Commun.*, vol. 17, no. 5, pp. 3386–3400, May 2018.

[5] L. D. Nguyen, H. D. Tuan, T. Q. Duong, and H. V. Poor, "Multi-user regularized zero-forcing beamforming," *IEEE Trans. Signal Process.*, vol. 67, no. 11, pp. 2839–2853, Jun. 2019.

[6] A. A. Nasir, H. D. Tuan, T. Q. Duong, H. V. Poor, and L. Hanzo, "Hybrid beamforming for multi-user millimeter-wave networks," *IEEE Trans. Veh. Technol.*, vol. 69, no. 3, pp. 2943–2956, Mar. 2020.

[7] S. Tretyakov, V. Asadchy, and A. Diaz-Rubio, "Metasurfaces for general control of reflection and transmission," in *World Scientific Handbook of Metamaterials and Plasmonics*. Singapore: World Scientific, 2017, ch. 6, pp. 249–293.

[8] C. Huang, A. Zappone, G. C. Alexandropoulos, M. Debbah, and C. Yuen, "Reconfigurable intelligent surfaces for energy efficiency in wireless communication," *IEEE Trans. Wireless Commun.*, vol. 18, no. 8, pp. 4157–4170, Aug. 2019.

[9] Q. Wu and R. Zhang, "Towards smart and reconfigurable environment: Intelligent reflecting surface aided wireless network," *IEEE Commun. Mag.*, vol. 58, no. 1, pp. 106–112, Jan. 2020.

[10] M. D. Renzo *et al.*, "Smart radio environments empowered by reconfigurable AI meta-surfaces: An idea whose time has come," *EURASIP J. Wireless Commun. Netw.*, vol. 2019, no. 1, p. 129, Dec. 2019.

[11] C. Huang *et al.*, "Holographic MIMO surfaces for 6G wireless networks: Opportunities, challenges, and trends," *IEEE Wireless Commun.*, vol. 27, no. 5, pp. 118–125, Oct. 2020.

[12] L. Yang, F. Meng, J. Zhang, M. O. Hasna, and M. D. Renzo, "On the performance of RIS-assisted dual-hop UAV communication systems," *IEEE Trans. Veh. Technol.*, vol. 69, no. 9, pp. 10385–10390, Sep. 2020.

[13] X. Liu, Y. Liu, and Y. Chen, "Machine learning empowered trajectory and passive beamforming design in UAV-RIS wireless networks," *IEEE J. Sel. Areas Commun.*, vol. 39, no. 7, pp. 2042–2055, Jul. 2021.

[14] S. Li, B. Duo, X. Yuan, Y.-C. Liang, and M. Di Renzo, "Reconfigurable intelligent surface assisted UAV communication: Joint trajectory design and passive beamforming," *IEEE Wireless Commun. Lett.*, vol. 9, no. 5, pp. 716–720, May 2020.

[15] L. Yang, X. Yan, D. B. da Costa, T. A. Tsiftsis, H.-C. Yang, and M.-S. Alouini, "Indoor mixed dual-hop VLC/RF systems through reconfigurable intelligent surfaces," *IEEE Wireless Commun. Lett.*, vol. 9, no. 11, pp. 1995–1999, Nov. 2020.

[16] L. Wei, C. Huang, G. C. Alexandropoulos, C. Yuen, Z. Zhang, and M. Debbah, "Channel estimation for RIS-empowered multi-user MISO wireless communications," *IEEE Trans. Commun.*, vol. 69, no. 6, pp. 4144–4157, Jun. 2021.

[17] J. He, H. Wymeersch, and M. Juntti, "Channel estimation for RIS-aided mmWave MIMO systems via atomic norm minimization," *IEEE Trans. Wireless Commun.*, early access, Apr. 7, 2021, doi: 10.1109/TWC.2021.3070064.

[18] Z. Zhang, C. Zhang, C. Jiang, F. Jia, J. Ge, and F. Gong, "Improving physical layer security for reconfigurable intelligent surface aided NOMA 6G networks," *IEEE Trans. Veh. Technol.*, vol. 70, no. 5, pp. 4451–4463, May 2021.

[19] M. H. Khoshafa, T. M. N. Ngatched, and M. H. Ahmed, "Reconfigurable intelligent surfaces-aided physical layer security enhancement in D2D underlay communications," *IEEE Commun. Lett.*, vol. 25, no. 5, pp. 1443–1447, May 2021.

[20] C. Huang, R. Mo, and C. Yuen, "Reconfigurable intelligent surface assisted multiuser MISO systems exploiting deep reinforcement learning," *IEEE J. Sel. Areas Commun.*, vol. 38, no. 8, pp. 1839–1850, Aug. 2020.

[21] Q.-U.-A. Nadeem, A. Kammoun, A. Chaaban, M. Debbah, and M.-S. Alouini, "Asymptotic max-min SINR analysis of reconfigurable intelligent surface assisted MISO systems," *IEEE Trans. Wireless Commun.*, vol. 19, no. 12, pp. 7748–7764, Dec. 2020.

[22] Q. Wu and R. Zhang, "Intelligent reflecting surface enhanced wireless network via joint active and passive beamforming," *IEEE Trans. Wireless Commun.*, vol. 18, no. 11, pp. 5394–5409, Nov. 2019.

[23] G. Zhou, C. Pan, H. Ren, K. Wang, and A. Nallanathan, "Intelligent reflecting surface aided multigroup multicast MISO communication systems," *IEEE Trans. Signal Process.*, vol. 68, pp. 3236–3251, Apr. 2020.

[24] C. Pan *et al.*, "Multicell MIMO communications relying on intelligent reflecting surfaces," *IEEE Trans. Wireless Commun.*, vol. 19, no. 8, pp. 5218–5233, Aug. 2020.

[25] C. Pan *et al.*, "Intelligent reflecting surface aided MIMO broadcasting for simultaneous wireless information and power transfer," *IEEE J. Sel. Areas Commun.*, vol. 38, no. 8, pp. 1719–1734, Aug. 2020.

[26] M.-M. Zhao, Q. Wu, M.-J. Zhao, and R. Zhang, "Intelligent reflecting surface enhanced wireless networks: Two-timescale beamforming optimization," *IEEE Trans. Wireless Commun.*, vol. 20, no. 1, pp. 2–17, Jan. 2021.

[27] H. Yu, H. D. Tuan, A. A. Nasir, T. Q. Duong, and H. V. Poor, "Joint design of reconfigurable intelligent surfaces and transmit beamforming under proper and improper Gaussian signaling," *IEEE J. Sel. Areas Commun.*, vol. 38, no. 11, pp. 2589–2603, Nov. 2020.

[28] S. Lagen, A. Agustin, and J. Vidal, "Coexisting linear and widely linear transceivers in the MIMO interference channel," *IEEE Trans. Signal Process.*, vol. 64, no. 3, pp. 652–664, Feb. 2016.

[29] A. A. Nasir, H. D. Tuan, T. Q. Duong, and H. V. Poor, "Improper Gaussian signaling for broadcast interference networks," *IEEE Signal Process. Lett.*, vol. 26, no. 6, pp. 808–812, Jun. 2019.

[30] H. D. Tuan, A. A. Nasir, H. H. Nguyen, T. Q. Duong, and H. V. Poor, "Non-orthogonal multiple access with improper Gaussian signaling," *IEEE J. Sel. Topics Signal Process.*, vol. 13, no. 3, pp. 496–507, Jun. 2019.

[31] H. Yu, H. D. Tuan, T. Q. Duong, Y. Fang, and L. Hanzo, "Improper Gaussian signaling for integrated data and energy networking," *IEEE Trans. Commun.*, vol. 68, no. 6, pp. 3922–3934, Jun. 2020.

[32] H. Yu, H. D. Tuan, A. A. Nasir, T. Q. Duong, and L. Hanzo, "Improper Gaussian signaling for computationally tractable energy and information beamforming," *IEEE Trans. Veh. Technol.*, vol. 69, no. 11, pp. 13990–13995, Nov. 2020.

[33] Ö. Özdogan, E. Björnson, and E. G. Larsson, "Intelligent reflecting surfaces: Physics, propagation, and pathloss modeling," 2019, *arXiv:1911.03359*. [Online]. Available: http://arxiv.org/abs/1911.03359

[34] E. Bjornson, O. Ozdogan, and E. G. Larsson, "Intelligent reflecting surface versus decode-and-forward: How large surfaces are needed to beat relaying?" *IEEE Wireless Commun. Lett.*, vol. 9, no. 2, pp. 244–248, Feb. 2020.

[35] Q.-U.-A. Nadeem, A. Kammoun, M. Debbah, and M.-S. Alouini, "A generalized spatial correlation model for 3D MIMO channels based on the Fourier coefficients of power spectrums," *IEEE Trans. Signal Process.*, vol. 63, no. 14, pp. 3671–3686, Jul. 2015.

[36] P. D. Tao and L. T. H. An, "A D.C. Optimization algorithm for solving the trust-region subproblem," *SIAM J. Optim.*, vol. 8, no. 2, pp. 476–505, May 1998.

[37] A. Migdalas, "A regularization of the Frank-and-Wolfe method and unification of certain nonlinear programming methods," *Math. Program.*, vol. 65, pp. 331–346, Feb. 1994.

[38] P. J. Schrerier and L. L. Scharf, *Statistical Signal Processing of Complex-Valued Data: The Theory of Improper and Noncircular Signals*. Cambridge, U.K.: Cambridge Univ. Press, 2010.

[39] E. Telatar, "Capacity of multi-antenna Gaussian channels," *Eur. Trans. Telecommun.*, vol. 10, no. 6, pp. 585–595, Nov. 1999.

Hongwen Yu received the B.S. and M.S. degrees in communication and information engineering from Shanghai University, Shanghai, China, in 2011 and 2014, respectively. He is currently pursuing the double Ph.D. degree with the School of Electrical and Data Engineering, University of Technology Sydney, Ultimo, NSW, Australia. His current research interests include optimization methods for wireless communication and signal processing.

Hoang Duong Tuan received the Diploma (Hons.) and Ph.D. degrees in applied mathematics from Odessa State University, Ukraine, in 1987 and 1991, respectively. He spent nine academic years in Japan as an Assistant Professor with the Department of Electronic-Mechanical Engineering, Nagoya University, from 1994 to 1999, and then as an Associate Professor with the Department of Electrical and Computer Engineering, Toyota Technological Institute, Nagoya, from 1999 to 2003. He was a Professor with the School of Electrical Engineering and Telecommunications, University of New South Wales, from 2003 to 2011. He is currently a Professor with the School of Electrical and Data Engineering, University of Technology Sydney. He has been involved in research with the areas of optimization, control, signal processing, wireless communication, and biomedical engineering for more than 20 years.

Eryk Dutkiewicz (Senior Member, IEEE) received the B.E. degree in electrical and electronic engineering and the M.Sc. degree in applied mathematics from the University of Adelaide in 1988 and 1992, respectively, and the Ph.D. degree in telecommunications from the University of Wollongong in 1996. In early 2000's, his industry experience includes management of the Wireless Research Laboratory, Motorola. He is currently the Head of School of Electrical and Data Engineering, University of Technology Sydney, Australia. He also holds a professorial appointment at Hokkaido University, Japan. His current research interests cover 5G/6G and the IoT networks.

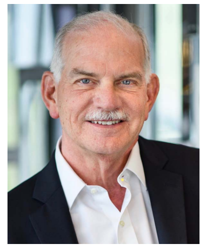

H. Vincent Poor (Life Fellow, IEEE) received the Ph.D. degree in electrical engineering and computer science (EECS) from Princeton University in 1977.

From 1977 to 1990, he was on the faculty of the University of Illinois at Urbana–Champaign. Since 1990, he has been on the faculty at Princeton, where he is currently a Michael Henry Strater University Professor. From 2006 to 2016, he was the Dean of Princeton's School of Engineering and Applied Science. He has held a visiting appointments at several other universities, including most recently at Berkeley and Cambridge. His research interests are in the areas of information theory, machine learning and network science, and their applications in wireless networks, energy systems, and related fields. Among his publications in these areas is the forthcoming book *Machine Learning and Wireless Communications* (Cambridge University Press, 2021). Dr. Poor is a member of the National Academy of Engineering and the National Academy of Sciences and a Foreign Member of the Chinese Academy of Sciences, the Royal Society, and other national and international academies. Recent recognition of his work includes the 2017 IEEE Alexander Graham Bell Medal.

Lajos Hanzo (Fellow, IEEE) received the master's and Ph.D. degrees from the Technical University (TU) of Budapest in 1976 and 1983, respectively, the Doctor of Sciences (D.Sc.) degree from the University of Southampton in 2004, the Ph.D. (Hons.) degree from TU of Budapest in 2009, and the Ph.D. degree (Hons.) from the University of Edinburgh in 2015. He has published more than 1900 contributions at IEEE Xplore, 19 Wiley-IEEE Press books, and has helped the fast-track career of 123 Ph.D. students. Over 40 of them are Professors at various stages of their careers in academia and many of them are leading scientists in the wireless industry. He is a Foreign Member of the Hungarian Academy of Sciences and the former Editor-in-Chief of the IEEE Press. He is also a fellow of the Royal Academy of Engineering (FREng), IET, and EURASIP. He has served several terms as a Governor of both IEEE ComSoc and VTS. (http://www-mobile.ecs.soton.ac.uk, https://en.wikipedia.org/wiki/Lajos_Hanzo).